NeuroMolecular Medicine
Copyright © 2007 Humana Press Inc.
All rights of any nature whatsoever reserved.
ISSN0895-8696/07/09:55–82/$30.00 (Online) 1559-1174
doi: 10.1385/NMM:9:1:55

ORIGINAL ARTICLE

Tryptamine Induces Tryptophanyl-tRNA Synthetase-Mediated Neurodegeneration With Neurofibrillary Tangles in Human Cell and Mouse Models

Elena L. Paley,*[,1,2] Galina Denisova,[3] Olga Sokolova,[4] Natalia Posternak,[2] Xukui Wang,[5] and Anna-Liisa Brownell[5]

[1]Department of Urology, Northwestern University Feinberg School of Medicine, Chicago, IL 60611; [2]Expert BioMed, Inc., Miami, FL 33179; [3]Department of Pathology and Molecular Medicine, Center for Gene Therapeutics, McMaster University, Hamilton, ON, Canada; [4]Howard Hughes Medical Institute and Department of Biochemistry, Brandeis University, Waltham, MA 02454; and [5]Department of Radiology, Massachusetts General Hospital, and Harvard University Medical School, Boston, MA 02114

Received December 3, 2004; Revised May 8, 2006; Accepted May 9, 2006

Abstract

The neuropathological hallmarks of Alzheimer's disease (AD) and other taupathies include neurofibrillary tangles and plaques. Despite the fact that only 2–10% of AD cases are associated with genetic mutations, no nontransgenic or metabolic models have been generated to date. The findings of tryptophanyl-tRNA synthetase (TrpRS) in plaques of the AD brain were reported recently by the authors. Here it is shown that expression of cytoplasmic-TrpRS is inversely correlated with neurofibrillary degeneration, whereas a nonionic detergent-insoluble presumably aggregated TrpRS is simultaneously accumulated in human cells treated by tryptamine, a metabolic tryptophan analog that acts as a competitive inhibitor of TrpRS. TrpRS-N-terminal peptide self-assembles in double-helical fibrils in vitro. Herein, tryptamine causes neuropathy characterized by motor and behavioral deficits, hippocampal neuronal loss, neurofibrillary tangles, amyloidosis, and glucose decrease in mice. Tryptamine induced the formation of helical fibrillary tangles in both hippocampal neurons and glia. Taken together with the authors' previous findings of tryptamine-induced nephrotoxicity and filamentous tangle formation in kidney cells, the authors' data indicates a general role of tryptamine in cell degeneration and loss. It is concluded that tryptamine as a component of a normal diet can induce neurodegeneration at the concentrations, which might be consumed along with food. Tryptophan-dependent $tRNA^{trp}$ aminoacylation catalyzed by TrpRS can be inhibited by its

*Author to whom all correspondence and reprint requests should be addressed. E-mail: elenapaley@cs.com; e-paley@nortwestern.edu

substrate tryptophan at physiological concentrations was demonstrated. These findings indicate that the dietary supplementation with tryptophan as a tryptamine competitor may not counteract the deleterious influence of tryptamine. The pivotal role of TrpRS in protecting against neurodegeneration is suggested, providing an insight into the pathogenesis and a possible treatment of neurodegenerative diseases.

doi: 10.1385/NMM:9:1:55

Index Entries: Alzheimer's disease; neurodegeneration; neurofibrillary tangles; tryptamine; tryptophanyl-tRNA synthetase.

Introduction

Tryptamine is a potent competitive inhibitor of tryptophanyl-tRNA synthetase (TrpRS) (Kisselev et al., 1979; Fromant et al., 1981; Lowe and Tansley, 1984), a phosphoprotein (Paley, 1997) induced by interferons in human cells (Rubin et al., 1991). TrpRS catalyzes the attachment of tryptophan to $tRNA^{trp}$ in the initial step of protein biosynthesis. As a close structural analog of tryptophan, tryptamine compete with tryptophan, with K_i 6×10^{-7} M when K_m for tryptophan is 0.9×10^{-7} M in tryptophan-dependent ATP-pyrophosphate exchange, an activation step of tRNA aminoacylation (Kisselev et al., 1979). In the authors' earlier study, tryptamine showed cytotoxic effect on bovine kidney Madin-Darby Bovine Kidney (MDBK) cells with Lethal $Dose_{90}$ of 30 µg/mL when tryptophan was at 5 µg/mL in the culture medium (Paley et al., 1991). The tryptamine to tryptophan ratio of 6 in the medium for the MDBK-cell cultivation is close to the ratio of K_i for tryptamine/K_m for tryptophan indicated earlier. This is apparently sufficient for the TrpRS inhibition and consequent death of majority of kidney cells sensitive to tryptamine. In MDBK cells that are resistant to tryptamine, the tangles of filaments with a diameter of 20 nm immunoreactive with monospecific antibodies to TrpRS were visualized by electron microscopy (Paley et al., 1991). These formations resemble morphologically the neurofibrillary tangles (NFT), the hallmarks of a number of neurodegenerative diseases including age-related Alzheimer's disease (AD) and Parkinson's disease (PD) (Spillantini and Goedert, 1998) and sporadic inclusion body myositis (Cherin, 1999). NFT are made up of paired helical filaments (PHF) with a diameter of 8–20 nm, whereas tau protein is the major protein of one form of PHF (Lee et al., 1991).

The aberrant protein aggregation is a characteristic pathological feature of neurodegenerative diseases (Mattson and Sherman, 2003). TrpRS and its peptides are very susceptible to aggregation (Paley et al., 2006). The N-terminal TrpRS peptide that can be proteolytically deleted in vivo is self-aggregated in cytotoxic fibrils in vitro. Furthermore, the aggregates resembling plaques were detected in AD brain with monoclonal and polyclonal antibodies to TrpRS (Paley et al., 2006). Tryptamine is a cell metabolite formed through tryptophan decarboxylation by aromatic amino acid decarboxilase. The aromatic amino acid decarboxilase level can be elevated under different conditions (Young et al., 1994; Gilbert et al., 1995) and such an increase can lead to the elevation of tryptamine level. Monoamine oxidases A and B (MAO) catalyze the conversion of tryptamine into indole-3-acetic acid with the formation of hydrogen peroxide (Mousseau, 1993; Adeghate and Parvez, 2004), whereas MAO inhibition leads to an increase in tryptamine level (Dewhurst, 1968). The MAO activity is changed in diabetes (Adeghate and Parvez, 2004), AD, and PD (Riederer et al., 2004). Tryptamine is a neuromodulator possessing plural physiological dose-dependent effects. The content of tryptamine in food and beverages are varied and significant in some foodstuffs and food-associated bacteria. The values determined for tryptamine are 298.5 mg/kg in chick pea and 567.3 mg/kg in lupine seeds following germination, a usual step in cooking (Shalaby, 2000), approx 25 mg/kg of goat cheese (Novella-Rodrigues et al., 2002), 50–100 mg/kg of a canned fish (Valls et al., 2002), 10 mg/L in a beer (Kalac and Krizek, 2003), approx 14 mg/kg in frozen spinach puree, approx 20 mg/kg in concentrated tomato pasta, approx 72 mg/kg in ketchup, approx 24 mg/kg in frozen green pea (Kalac et al., 2002), 5 mg/kg of tomato, 5.2 mg/kg of kiwi (Tsuchiya et al., 1995), and 4–9 mg/kg of pomegranate and strawberry (Badria, 2002).

The bacteria *Lactobacillus curvatus* produces tryptamine at 1321 mg/L of broth. This bacteria most

commonly found in the meat and meat products such as fermented sausages (Bover-Cid et al., 2001) is also found in humans (Walter et al., 2001) and even causes a bacteremia (Arpi et al., 2003). The *Staphylococcus xylosus* isolated from fermented sausages produces tryptamine at 10–15 mg/L of medium (Martuscelli et al., 2000) and approx 127 mg/kg of tryptamine was detected in Turkish sausages (Erkmen and Bozkurt, 2004). More factors regulating tryptamine levels in humans are related to its transport. Tryptamine can use the same monoamine transporter as the neurotransmitters serotonin, dopamine, and histamine, although the recognition of each of the ligands involves independent interactions with the transport protein (Flinn and Edwards, 1998). Tryptamine is directed to specific receptor(s) in the human brain (Mousseau and Butterworth, 1994; Lewin, 2006) and can easily cross the blood–brain barrier (Mousseau, 1993). The possible competitive inhibitory tryptamine effect depends on the level of tryptophan, an essential amino acid required for the survival of humans. A number of factors control the level of tryptophan in a cell. One of them is indoleamine 2,3-dioxygenase catalyzing the conversion of tryptophan to *N*-formylkynurenine.

The indoleamine 2,3-dioxygenase expression is upregulated by interferon and influenza virus (Taylor and Feng, 1991). For the transport across the blood–brain barrier through large neutral amino acid transporters, the tryptophan competes with other large neutral amino acids present usually at higher concentrations than tryptophan in the extracellular brain fluid (O'Kane and Hawkins, 2003). Tryptophan is a least available amino acid in food (Bremer et al., 1996). In contrast to other large neutral amino acids, the total tryptophan level, which includes both free and bound tryptophan is significantly lower in the older than in younger population from both sexes (Demling et al., 1996). In the same work, the free-tryptophan content in normal human plasma of 5.5 µ*M* (approx 1.3 mg/L) in males and 5.9 µ*M* in females was similar in younger and older groups. It should be noted that concentration of a bound tryptophan is about 10 times more than the content of a free tryptophan in human plasma, although only free tryptamine was estimated. The tryptophan plasma level is decreased in patients with PD (Molina et al., 1997) and early-stage probable AD (Fekkes et al., 1998). On the other hand, tryptophan depletion leads to depression (Newmester et al., 1999), which is common in elderly people (Rowe and Rapoport, 2006), patients with PD (McDonald et al., 2006), and is associated with 52% of AD cases (Starkstein et al., 2005). Moreover, acute tryptophan depletion resulted in impairment on tasks of working memory in healthy elderly (Porter et al., 2003).

It was hypothesized that tryptophan decrease accompanied by increased or even unchanged tryptamine levels in cells might result in an increase of the tryptamine to tryptophan ratio to make it sufficient for the TrpRS inhibition. Half-life for tryptamine in the mouse brain is 0.9 min (Jurio and Durden, 1984), whereas a half-life of fluoro-trytophan in the rat brain was estimated at 0.5–1 h (Chanut et al., 1993). Despite the short half-life, the concentration of tryptamine can be high within a short period of time as a result of its high turnover (Mousseau, 1993). The major metabolite of tryptamine indol-3-acetic acid was elevated in cerebrospinal fluid of retarded depressives (Anderson et al., 1984). The increased urinary tryptamine excretion (Sullivan et al., 1980) and higher in vitro ^{14}C-tryptamine half-life in blood (Domino and Gahagan, 1977) were observed in chronic schizophrenics. The density of [^{3}H]tryptamine binding sites in frontal cortex, hippocampus, and caudate nucleus of the brain tissue from patients with hepatic encepholopathy was significantly decreased in comparison with control brain tissue (Mousseau and Butterworth, 1994). The decreased binding can be result of tryptamine increase in the brain zones. However, as a result of a postmortem delay time of 16–17 h and a very short half-life of tryptamine, these data are difficult to interpret. It is proposed that, although tryptamine can prevail the tryptophan content in cells within a short period of time, it can be sufficient for an inhibition of tryptophan incorporation into proteins leading to cell death. Whether tryptamine indeed has a neurotoxic effect and induces NFT is unknown. The multiple effects of tryptamine at physiological concentrations on human neuronal cells and mouse brain were studied.

Materials and Methods

Tryptamine Treatment of Cells

SH-SY5Y human neuroblast cells (Biedler et al., 1973) were obtained from the Cell Culture Facility, Weizmann Institute of Science, Israel. The cells were grown on 25 cm^2 flasks (TPP, Switzerland) with 5%

CO_2 at 37°C in RPMI 1640 medium supplemented with 10% fetal calf serum, 100 U/mL penicillin, 100 µg/mL streptomycin, 0.25 µg/mL amphoterycin, and 2 m*M* glutamine. The epithelial-like enriched cells were selected from SH-SY5Y cells and then treated with 20–100 µg/mL of tryptamine for 6–60 d.

Immunostaining of Neuronal Markers

The SH-SY5Y epithelial-like cells grown as monolayer were washed in phosphate-buffered saline (PBS), fixed in a freshly prepared fixative of 4% formaldehyde (Merck, NJ), 0.25% glutaraldehyde (Sigma, St. Louis, MO; for electron microscopy) in PBS, pH 7.2 for 30–45 min at room temperature. It was then incubated with 0.15% saponine in PBS for 30 min, 2% hydrogen peroxide in 50% methanol for 30 min, and then with 0.5 mg/mL sodium borohydride for 5 min. After washing, the specimens were blocked with 2% bovine serum albumin (BSA) (Immunoglobulin [Ig]G-free, protease-free, Jackson IRL, PA) for 20 min and then incubated with monoclonal antibody (MAb) against synaptophysin (dilution 1:100, initial concentration 50 µg/mL, clone SY38, ICN, Biomedicals Inc., OH), cocktail of MAbs against glial fibrillary acidic protein, clones 4A11, 1B4, and 2E1 (dilution 1:50, initial concentration 0.5 mg/mL, PharMingen, CA), purified mouse MAb against 160-kDa neurofilament protein, clone NN-18 (dilution 1:50, initial concentration 0.1 mg/mL, Calbiochem-Novabiochem International, catalog no. ASK16), and rabbit-polyclonal antibody to neuronal-specific enolase (NSE, γ/γ isoenzyme) of human brain (prediluted by manufacturer, Ab-1, Calbiochem) overnight at 4°C. After washing five times with PBS, cells were incubated with peroxidase-conjugated $F(ab')_2$ fragment goat antimouse (1:500 or 1:1000), antirabbit IgG $F(ab')_2$ fragment specific (1:100), and Cy 3-conjugated $F(ab')_2$ fragment goat antimouse IgG $F(ab')_2$ fragment specific diluted 1:300 (Jackson) for 1 h at room temperature. For peroxidase staining, cells were incubated with mouse $F(ab')_2$ peroxidase–antiperoxidase (PAP; Jackson, 1:600) for 1 h at 37°C and then washed five times with PBS. Peroxidase reaction was developed with diaminobenzidine. For immunofluorescent labeling, pretreatment with hydrogen peroxide and sodium borohydride was omitted and cells were incubated directly with fluorescent antibodies. To examine the specificity, the cells were incubated with only secondary antibodies and PAP. After immunostaining, cells were counterstained with hematoxylin and were examined under phase-contrast microscope attached to a camera (Olympus, Japan) following by digital scanning with DiMAGE Scan Multi II (Minolta, UK), DiMAGE scan software, and Adobe Photoshop 7.0, or visualized with confocal laser-scanning microscope (Zeiss, Germany).

Immunofluorescence

The control and tryptamine-treated cells fixed as above were incubated with 1% Triton X-100 for 7 min and then washed with PBS. Then cells were double-labeled with mouse anti-PHF-tau MAb (clone AT8, Innogenetics, Ghent, Belgium, 1:25 or 1:50 dilution) and previously characterized polyclonal anti-TrpRS antibodies diluted 1:100 or incubated with MAbs to TrpRS (Paley et al., 2006) in 0.15% saponine in PBS, 0.5% BSA (IgG-free, protease-free, Jackson), 0.1% sodium aside, 2 m*M* PMSF overnight at 4°C. After washing with PBS, the cells were incubated with Cy 3-conjugated $F(ab')_2$ fragment goat antimouse IgG $F(ab')_2$ fragment specific (Jackson, 1:800) and FITC-conjugated goat antirabbit IgG (Sigma, 1:100) for 1 h at 37°C. After washing, the cells were examined with fluorescent microscope attached to the image windows software (Leica, Germany). The specificity control included incubation with anti-TrpRS antibodies depleted with excess of recombinant purified hTrpRS as described (Paley et al., 2006). The immunolabeled cells were routinely counterstained with hematoxylin and examined under phase-contrast microscope as described in the previous section.

Electron Microscopy of Cells

The control and tryptamine-treated cells grown as monolayer were washed in PBS, incubated with fixative as described in the previous section, washed with PBS at 4°C, and then collected with scraper (Greiner, Longwood, FL) or rubber policeman. After centrifugation, the cells were transferred to 0.1 *M* cacodylate buffer, pH 7.2, postfixed in 1% OsO_4 in the same buffer for 1 h, washed and dehydrated in series of alcohols, and then in propylenoxide. Specimens were polymerized in propilenoxide/Epon-812 or only Epon-812. Ultrathin sections (70–90 nm) were placed on 300-mesh Ni grids. For immunolabeling, some grids were washed with saturated methaperiodate for 60 min. The grids were blocked using 0.5% BSA, 1% gelatin, 1% Tween-20, and 1% glycine for 20 min, and then incubated with anti-TrpRS rabbit-polyclonal antibodies or mouse MAb AT8 (dilution 1:20) against

epitopes containing phosphorylated Serine 202/Threonine 205 (Innogenetics) overnight at 4°C. After washing, sections were incubated with 10-nm-colloidal gold-conjugated goat antirabbit IgG antibodies or 10-nm gold-conjugated antimouse antibodies (Zymed, CA, 1:20) for 1 h. Control specimens were incubated with secondary antibodies or with anti-TrpRS antibodies depleted with excess of purified hTrpRS as described earlier (Paley et al., 1991, 2006). The dried grids were examined using electron microscopes Philips EM-410 and CM-12 at 100 kw after postfixation with 2% uranylacetate and lead citrate for 5 min or without postfixation. In some experiments, the cells grown on 35-mm dishes (BD Falcon, USA) were fixed with 4% paraformaldehyde, 1.25% glutaraldehyde, PBS, pH 9.5 for 45 min, immunostained with PAP, and then processed for electron microscopy as a monolayer as described in Paley et al. (1991).

Total Cell Sodium Dodecyl Sulphate Extracts

Control and tryptamine-treated epithelial-like cells were washed with PBS, solubilized *in situ* in buffer containing 2% sodium dodecyl sulphate (SDS), 50 m*M* Tris-HCl, pH 6.8, and 100 m*M* dithiothreitol (100 µL of buffer per 5-cm plate), collected, and boiled for 5 min.

Triton Extraction

The epithelial-like cells were lysed in 0.1 *M* HEPES buffer, pH 6.9, 0.5% Triton X-100, 1 m*M* $MgCl_2$, 0.1 m*M* ethylenediaminetetraacetic acid (EDTA), 2 m*M* ethylene glycol *bis*(2-aminoethyl ether)-*N,N,N'N'*-tetracetic acid (EGTA), 1 m*M* dithiothreitol (DTT), 1 m*M* PMSF, 0.4 mg/mL aprotinin, 0.1 mg/mL antipain, leupeptin, pepstatin, and hemastatin, 0.1 µ*M* okadaic acid, 10 m*M* sodium ortovanadate, and 50 m*M* sodium fluoride *in situ* (1 mL of buffer per 8-cm plate) for 20 min at room temperature. Detergent-insoluble fraction was collected with scraper, washed in the same buffer excluding inhibitors of phosphatases, solubilized in SDS-sample buffer at 100°C for 5 min and then centrifuged.

Western Blotting

The equal amounts of extracts from control and treated cells were run in 10% SDS Laemmli polyacrylamide gel electrophoresis (PAGE), transferred onto nitrocellulose or polyvinylidene fluoride (PVDF) membranes, blocked in 5% nonfat dry milk, incubated with hybridoma supernatants (1:5) of MAb B1 to bTrpRS (clone 6C10) mapped to a region DDDKLEQIRRDYTSGAA close to the C-terminus of hTrpRS (Paley et al., 2006), with anti-p-tau AT8 anibody (1:50; Innogenetics) or with antibodies to neuronal markers for 1 h, washed with PBS, 0.1% Tween-20, probed with horseradish peroxidase-conjugated antimouse IgG and developed with ECL (Amersham Biosciences) or TMB (KPL Inc., Maryland) reagents. Kaleidoscope prestained markers (Bio-Rad, CA) were used for electrophoreses.

Aminoacylation of tRNA

The SH-SY5Y cells were washed twice with PBS, collected by scraper, and then centrifuged. The cells were lysed by quick freezing–thawing in the buffer of 50 m*M* HEPES, pH 7.4, 50 m*M* KCl, 2 m*M* $MgCl_2$, and cocktail of protease inhibitors (Roche Molecular Biochemicals), one tablet per 3–5 mL of the buffer. The lysate was centrifuged at 7500*g* in minicentrifuge at 0°C and the supernatant was used for reaction of tRNA aminoacylation. The reaction mixture contained [^{3}H]tryptophan (Amersham Pharmacia Biotech), specific activity 33 Ci/mmol or [^{3}H]glutamic acid (NEN Brand Radiochemicals, Perkin-Elmer, USA), 44 Ci/mmol. The labeled amino acids were added at 0.5 µCi to 100-µL reaction mixtures containing: 250 m*M* Tris-HCl, pH 7.5, 5 m*M* ATP, 5 m*M* $MgCl_2$, 0.2 m*M* EDTA, 0.2 mg/mL bovine serum albumin, and 2 mg/mL rabbit-liver total tRNA. The activity was measured at different concentrations of tryptophan and glutamic acid in the reaction mixtures of 0.1 µ*M*, 0.01 m*M*, 0.05 m*M*, 0.1 m*M*, and 0.5 m*M*. The amounts of crude cell extract in different experiments were 6, 10, and 17 µg in 100-µL incubation mixture. Incubation in different experiments was for 10, 15, 20, 30, and 35 min at 37°C. Incubation of the control sample containing all compounds for aminoacylation was at 0°C and terminated immediately. Reactions were stopped by adding 10% trichloroacetic acid.

TrpRS Synthetic Peptide

The synthesis, self-assembly, and electron microscopy analysis of a TrpRS-derived N-terminal peptide was conducted as described in Paley et al. (2006).

Acute Tryptamine Treatment of Mice

The protocol developed for acute tryptamine treatment enabled to analyze the change in a mouse

brain histochemically and electron microscopically in about a month after beginning of the treatment. The Balb/c mice were used for all studies in this research article. The male mice of weight of about 25 g at 8 wk of age were housed with free excess to water and food, a palleted chow diet (diet no. 19510, Koffolk, Israel) with 21% total protein, containing approx 2 mg of total tryptophan per day (approx 0.2 mg of free tryptophan). To determine a nontoxic dose, tryptamine (hydrochloride form) at the dozes 1, 5, 10, 50, 100, 500, and 1000 μg per mouse in PBS was injected intravenously in tails for every second day. No toxic effect of the dozes 1–500 μg was visible within 48 h after each injection. However, the mice had convulsions in 1–3 min after injections of 1 mg of tryptamine and then were sleepy. After 2 wk of stepwise intravenous injections, tryptamine was injected intraperitoneally. Each injection of 200 μg of tryptamine in 0.2 mL of noncomplete adjuvant for 2.5 wk was administered for every second day. Until the end of the experiments, the tryptamine mice were in good health and visibly gained more weight than the control mice. For histochemistry, brains were isolated from three control mice injected with placebo and three tryptamine-treated mice.

Histochemistry of Brain Sections and Counting the Neurons

The brains of mice were fixed in 4% formaldehyde (Merck), 0.25% glutaraldehyde (Sigma), PBS, pH 7.0 for overnight, washed, and dehydrated. Paraffin-embedded 4-μm sections were processed for staining, deparaffinized in xylene, and hydrated. After washing with PBS, sections were routinely stained with hematoxylin or Highmann's Congo red for 10 min and Harris' hematoxylin for 2 min or silver stained according to Gallyas, 1970, mounted and examined under phase-contrast and polarized light. Manual counting was used to count hematoxylin stained neurons within hippocampal areas CA1, CA3–4, and dentate girus (DG) using light microscope Olympus CK40 (Japan) interfaced with color camera and a digital scanner Konica Minolta DiMAGE Scan Multi II interfaced with computer. DiMAGE image software package was used to generate the microscopic images on the monitor for individual signal counting. Although, the stereology counting results in a higher number of neurons across groups we chose to count neurons manually instead of stereoscopically because the trend of reduction of neurons on treatment was found to be consistent with either method (Sari and Zhou, 2004). All analyses are derived from 20 hippocampal sections of three to four tryptamine$^+$ and three to four normal mice under the same dietary conditions for each experiment.

Electron Microscopy of Hippocampal Sections

The semi-thick sections of the whole mouse brains embedded into paraffin were rehydrated and stained as described in the previous section with hematoxylin and examined under the light microscope to identify areas of interest. The hippocampal areas were cut out from the paraffinized blocks with the razor blade into smaller pieces (1×1 mm^2), processed as above then postfixed with 4% osmium tetroxide in 0.2% Na cacodylate for 1 h at 4°C, *en block* stained with uranyl acetate, dehydrated with ethanol and propylene oxide, and embedded into Embed-812/Araldite-502. The ultrathin sections were applied onto formvar-coated 200-mesh copper grids, stained with lead citrate and examined in Morgagni 268 electron microscope at 80 kV. Photographs were taken at 45,000 and 90,000 magnification and analyzed (Sokolova et al., 2003).

Behavioral Experiments

Tryptamine in PBS at 50 μg per mouse has been injected intraperitoneally in 10 male mice at 8 wk of age, once a week for 5 mo and then mice have been observed without injections for 3 mo. The control 10 mice were injected with a placebo. All mice were in a good condition until the end of the experiments. Behavior of mice was examined on sticks after 3, 4, and 5 mo of injections. The mice were put on a narrow metallic stick of 1 cm in diameter and 80-cm long that was adjusted 30 cm above the platform. Time of their stable sitting and running on the stick as well as a percent of the way that was completed without a fall were measured. After 5 mo of injections followed by an interval of 1 mo without injections, the same mice were examined in swimming experiments. It was reported earlier that Balb/c mice showed a poor learning performance in the water maze task (Yoshida et al., 2001). It was also demonstrated that Balb/c mice fatigued during the learning period and it was suggested that the swimming exercise fatigue impaired learning efficiency in the Morris water maze (Mizunoya et al., 2004). Therefore, we used partly the elements of the

Morris water maze to examine effect of tryptamine on physical fatigue produced by swimming exercises of mice. The mice were individually labeled. The pool of 90 or 50 cm (pretraining) in diameter was made opaque by addition of milk to water. A transparent glass platform (9×9 cm^2) was submerged beneath the surface of water (2 cm). Each mouse was swimming three times a day with intersession intervals of 30–60 min. In each session, the mouse was allowed to swim until it found the platform. The mice were swimming repeatedly to navigate to a hidden platform of a fixed location of four trials until completing 12 trials. Mean swim time was calculated.

Treatment of Mice for Glucose Detection and Positron Emission Tomography Imaging

Male mice (8 wk of age, body weight 23–26 g) were purchased from the Charles River Laboratories (Wilmington, MA). The mice were housed three per cage under standard conditions with free access to food and water. The mice were randomized and handled under the same conditions by one investigator. In total, 12 mice were studied. Health of the animals and weight progression were closely monitored. All experiments were performed in compliance with the National Institutes of Health Guide for the Care and Use of Laboratory Animals and were approved by the Institutional Policy by the Subcommittee on Research Animals of the Harvard Medical School and Massachusetts General Hospital. Tryptamine-induced effect on glucose metabolism was investigated in six mice. Tryptamine (tryptamine hydrochloride, Sigma) was dissolved in PBS and prepared fresh for daily through intraperitoneal injection. The selected tryptamine dose was 200 μg per mouse for 22 d during 4 wk followed by an interval of 4 wk and another injection period of 6 d with the dose of 400 μg per mouse. As methodological control for the six tryptamine mice were administered with PBS with the same frequency as tryptamine injections.

Positron Emission Tomography

Imaging studies of glucose metabolism were conducted using 2-(18F)-fluoro-2-deoxy-D-glucose (^{18}F-FDG) as a tracer. ^{18}F-FDG was prepared with an automated robotic system attached to the cyclotron and based on the synthesis of Hamacher (Hamacher et al., 1986). For imaging studies, animals were anesthetized with isoflorane/N_2/O_2 anesthesia (1–1.5% isoflorane). Catheterization of tail vein was performed for injection of the labeled ligand and a blood sample was collected from the tail tip to determine blood glucose value. The animals were adjusted into a stereotactic headholder and into the imaging position in the positron emission tomography (PET) scanner; Concorde Microsystems microPET scanner (Model P4; Concorde Microsystems Inc., Knoxville, TN). For correction of attenuation a separate imaging was done using external rotating ^{68}Ge pin before injection of radioactivity. After injection of the radioactive ligand (100 μCi), volumetric data were acquired for 60 min in the list mode. Histograms were processed with appropriate corrections for uniformity, sensitivity, attenuation, decay, injected activity, and acquisition time. PET images were reconstructed using filtered back projection and Ramp filter with a cut-off value of 0.5. For analyses of data, regions of interest including left and right striatum, cingulate cortex, hippocampus, olfactory area, and cerebellum were drawn on several coronal brain levels (thickness of 1.25 mm). Glucose utilization was estimated from the measured time-activity curves at the steady state level (40 min after administration of the ligand). The average percent activity of the injected radioactivity (time interval 40–60 min) was corrected for the animal weight to obtain standardized unit values.

Results

Human Neuronal Cultured Cells

Effect of tryptamine on human neuroblastoma SH-SY5Y cell line was examined. This line includes two morphologically distinct cell types: predominantly fast dividing neuroblastic bearing short neurites, and significantly slower dividing epithelial-like lacking neuritis (Biedler et al., 1973). Following cultivation with 50–100 μg/mL tryptamine or tryptophanol for 5 d at initial density of 1×10^3 on 10-cm dishes in the medium, containing 5 μg/mL of tryptophan, all the cells died. Tryptamine from different manufactures produced similar cytotoxic effect. Continuous treatment with tryptamine at lower concentrations led to accumulation of large flattened, tightly substrate adherent epithelial-like

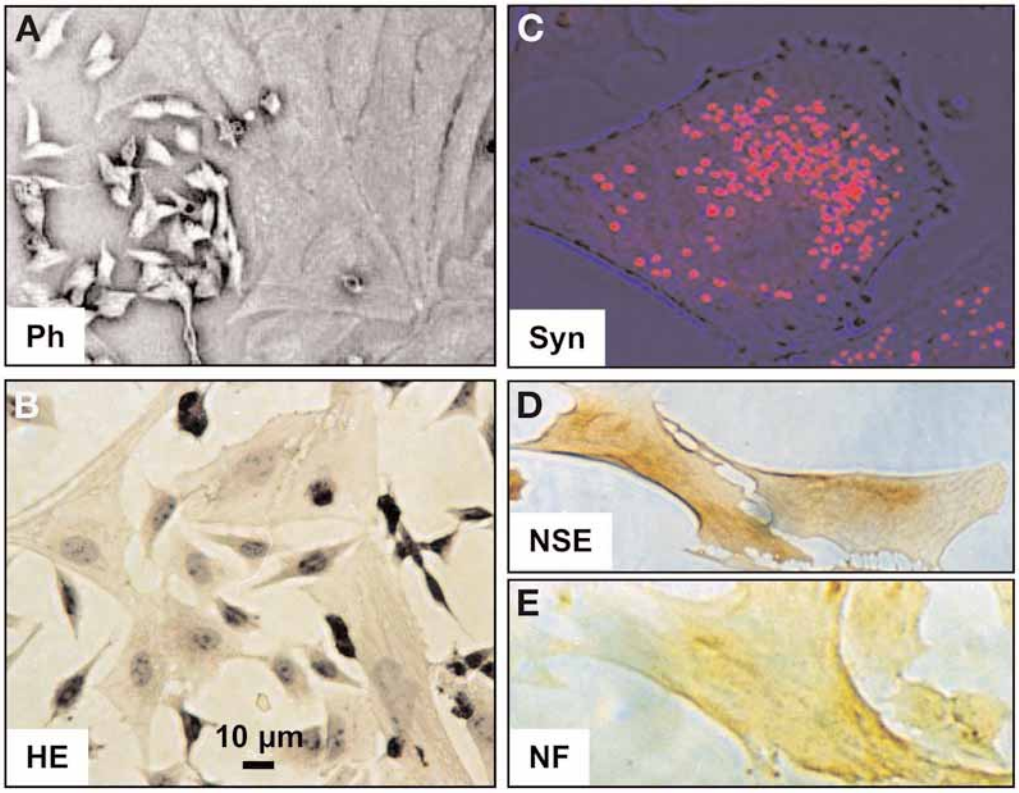

Fig. 1. Microscopy of human neuronal cells. **(A)** Phase-contrast (Ph) microscopy of SH-SY5Y cells enriched with epithelial-like cells. **(B)** Similar cells culture stained with hematoxylin. **(C)** Confocal fluorescent microscopy of epithelial-like cells with MAb to synaptophysin (Syn) and secondary antibodies labeled with Cy3 (red staining). **(D)** Peroxidase immunostaining of epithelial-like cells with antibodies to neuronal-specific enolase (NSE). Note the epithelial-like cells lacking processes show the outgrowth of processes following tryptamine treatment. **(E)** Peroxidase staining of epithelial-like cells with MAb to neurofilament M protein.

cells lacking neurites, whereas, the majority of neuroblasts died (first method of selection). To examine further the epithelial-like cells (Fig. 1) as less sensitive to tryptamine were chosen. Epithelial-like cells the separated from neuroblasts by exploiting a marked difference in adhesive properties. The weakly adherent neuroblasts were washed out with trypsin (second method of selection). The epithelial-like cells can be also accumulated in the "old" untreated culture (Fig. 1A,B) surviving without regular passages (third method of selection). The selected epithelial-enriched cells were treated further with 20–100 μg/mL tryptamine for 6–60 d. The epithelial-like cells with well-characterized antibodies to neuronal markers was first examined. The epithelial-like cells showed immunoreactivty with antibodies to synaptophysin (Fig. 1C), a synaptic vesicle marker, to neuronal-specific enolase (Fig. 1D) and to neurofilament protein of 160 kDa (Fig. 1E). The majority of cells did not show immunoreactivity with MAbs to glial fibrillary acidic protein (data not shown). Immunoblotting with specific antibodies revealed a predominant band corresponding to molecular mass of the neuronal markers (data not shown). Altogether the data confirmed the neuronal origin of the epithelial-like cells.

The control and tryptamine-treated epithelial-like cells were examined using both immunofluorescence (Fig. 2A–F) and immunoperoxidase (Fig. 2G,H) staining with MAb 6C10 and polyclonal antibodies to TrpRS as well as MAb AT8 to phosphorylated Tau. The manifestations resembling NFT (Fig. 2H) were detected in about 50% of tryptamine-treated cells and occasionally in old untreated culture using both anti-TrpRS antibodies (Fig. 2G) and AT8 (data not shown). It should be noted that NFT are frequently present in brains of aged nondemented people

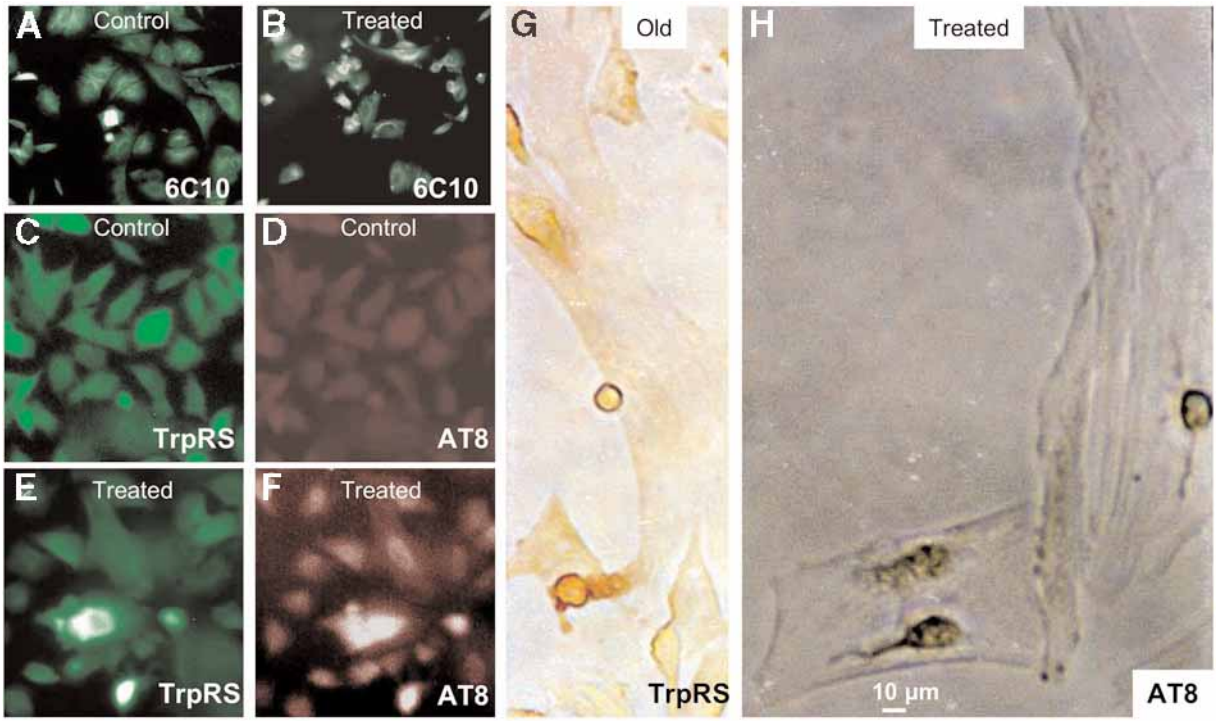

Fig. 2. Immunostaining of control and tryptamine-treated cells. **(A,B)** Immunofluorescence of control (C) and treated cells using MAb 6C10 to TrpRS (Paley et al., 2006). **(C–F)** Immunofluorescent double-labeling of control and treated cells with characterized rabbit polyclonal antibodies to TrpRS (TrpRS, 1:100) and MAb to p-tau AT8 at 1:50 (initial concentration 0.2 mg/mL) with addition of protease inhibitor 2 m*M* PMSF. Secondary antibodies were Cy3-conjugated (anti-mouse, 1:800, red) and FITC-conjugated (antirabbit, 1:100, green). **(G,H)** Immunoperoxidase staining of epithelilal-like cells (old cell culture) with antibodies to TrpRS (g) and AT8 MAb (treated cells).

(German et al., 1987; Gomez-Ramoz and Moran, 1998). The TrpRS and p-tau (AT8) immunoreactivity is partly colocolized in fluorescent double-labeled tryptamine-treated cells (Fig. 2E,F). Then both p-tau and TrpRS were examined by Western blotting. TrpRS is moderately decreased in the "cytoplasm" of the total cell extract and detergent-soluble fraction, whereas, its increase was found in the detergent-insoluble ("cytoskeleton") fraction (Fig. 3). The detergent-insoluble fraction includes the aggregated proteins. The p-tau was analyzed by Western immunoblot with AT8 antibody. The immunoblot pattern of cell extracts solubilized with SDS (Fig. 3) is similar to imunoblots developed with AT8 MAb using extracts obtained from normal and AD brain under similar conditions of protein solubilization in SDS-containing buffer (Huang et al., 2001), that is, large complexes (>220 kDa) were predominantly detected in the SDS-extracts. An increase of SDS-resistant oligomeric p-tau of 116 kDa is detected in tryptamine-treated cells. The SDS-resistance is about 100–220 kDa p-tau attributed previously as p-tau polymers was also detected in the brains of the high-expresser apoE4 mice by Western blotting with AT8 MAb (Harris et al., 2003). In PC12 neuronal cells besides of the monomeric 68 kDa tau, the high-molecular weight tau forms of 112 kDa were also found (Davis and Johnson, 1999). The high-molecular p-tau of more than 201 kDa was overexpressed in Triton-insoluble fraction of tryptamine-treated cells (Fig. 3). The p-tau from detergent-insoluble fraction of treated cells has higher molecular weight than p-tau from insoluble fraction of control epithelial-like cells. The appearance of higher molecular weight tau can be result of increase in its phosphorylation following tryptamine treatment.

Both untreated and tryptamine-treated cells were analyzed by electron microscopy. The representative images of untreated SH SY5Y neuronal cells show no filamentous tangles (Fig. 4A,B). In contrast, electron microscopy of tryptamine-treated cells visualizes

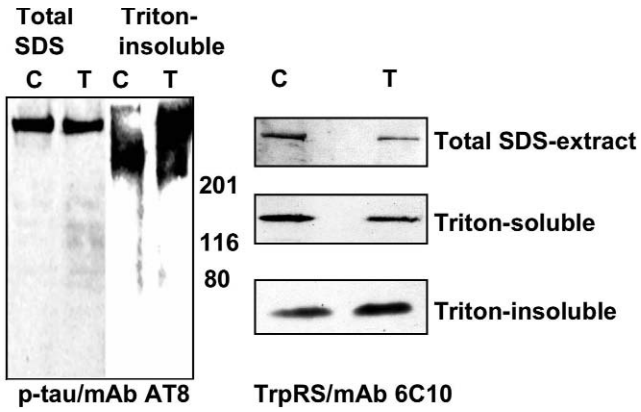

Fig. 3. Western immunoblotting of TrpRS and p-tau. Western blotting of SDS-total cell extract, detergent-soluble, and detergent-insoluble cell fractions from control (C) and tryptamine-treated (T) cells with anti-TrpRS MAb 6C10 (right panel) used as a hybridoma supernatant (1:5) and MAb AT8 (1:50). Treatment for detergent-soluble and detergent-insoluble extracts was performed at 20 µg/mL of tryptamine for 1 mo and for total extracts at 40 µg/mL for 4 d following by 20 µg/mL for 2 d. The equal amounts of proteins (about 80 µg/lane) of the epithelial-enriched extracts from control and tryptamine-treated cells were loaded on SDS-PAGE. The quantitative analysis of the proteins was performed using Coomassie blue and Ponceau staining of gels and blots.

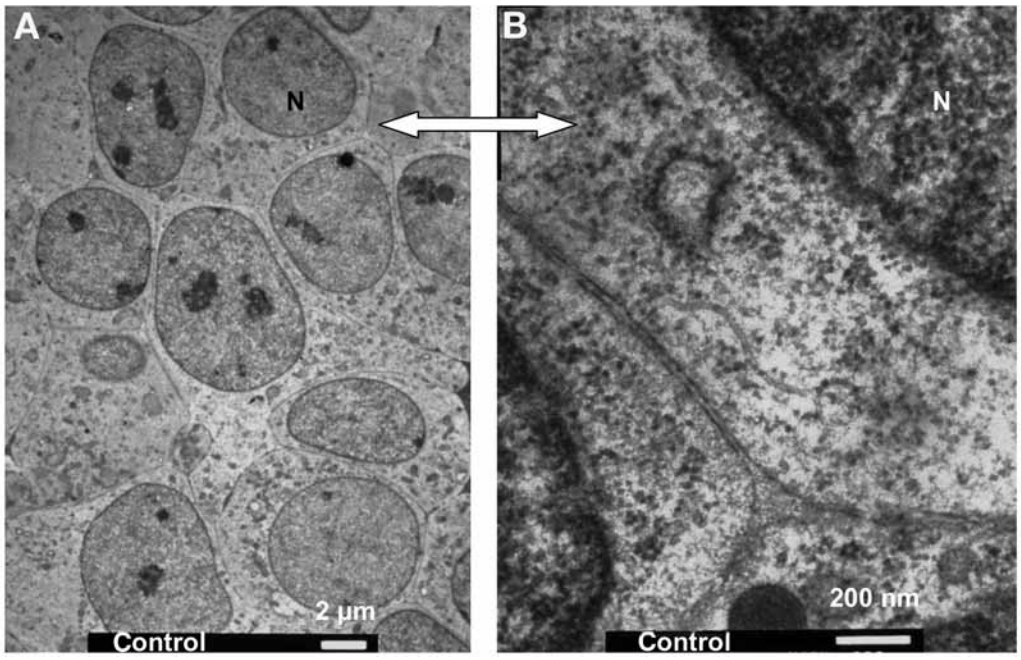

Fig. 4. *(Continued)*

numerous tangles made up of twisted and PHF (Fig. 4), moreover some cells contain more than one NFT (Fig. 4C,F). The Fig. 4C–H include at least six different cells with intracellular NFT made up of PHF and Fig. 4I–K visualize apparently extracellular NFT. The panel 4H shows a high magnification of helical fibrils with a diameter of about 24 nm and a helix periodicity of about 97 nm. The numerous helical fibrils with a diameter of about 8 nm and a helix periodicity of about 16–20 nm or without apparent

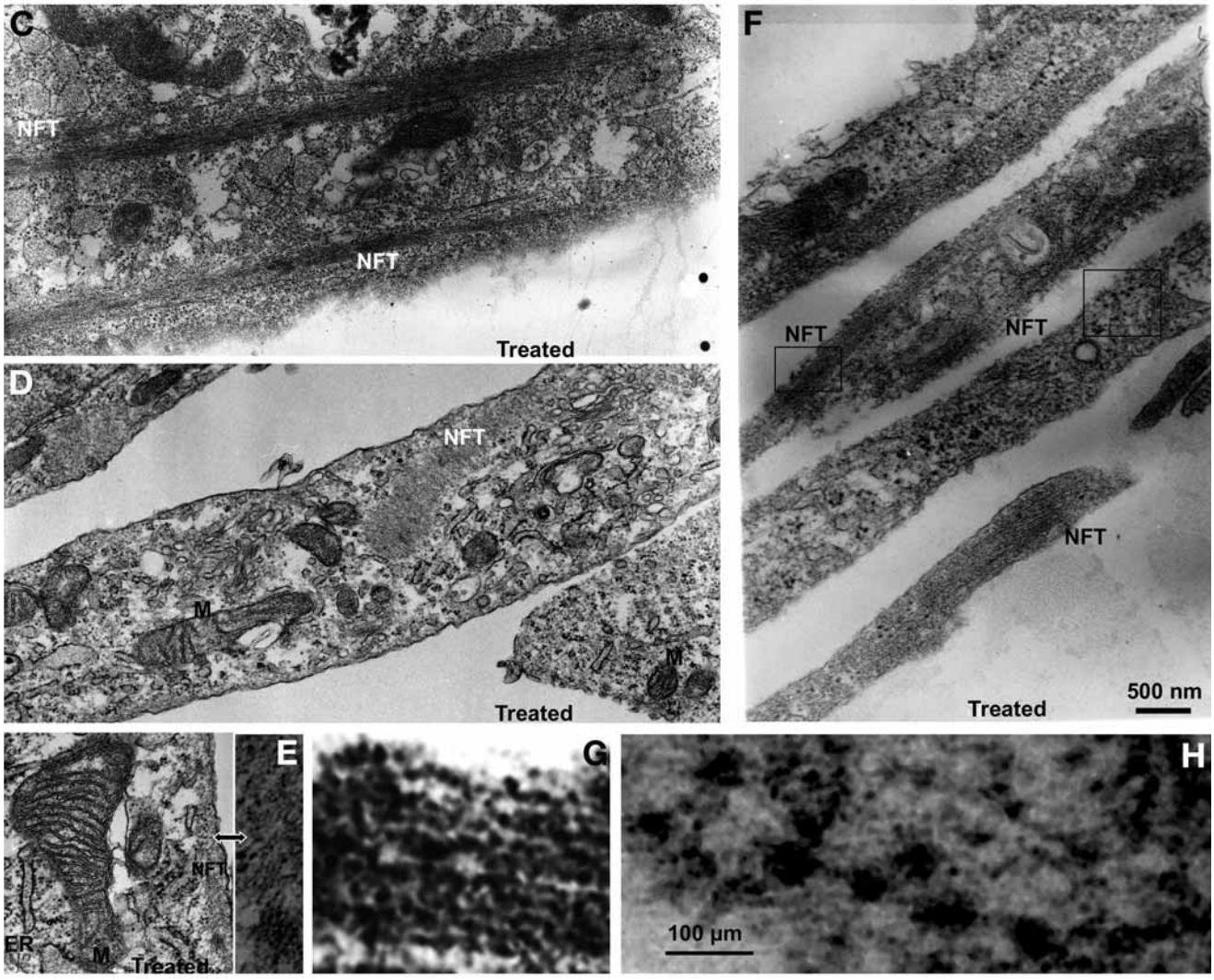

Fig. 4. *(Continued)*

periodicity are shown on Fig. 4E,G. Note the NFT of AD contain PHF with a diameter of 8–20 nm and a helix periodicity of 80–100 nm (Tabaton et al., 1991). The image on Fig. 4I shows remains of presumably dead cell located close to the intact cell. The dead cell contains inclusions with densely packed paired helical fibrils of a diameter of about 10–12 nm and a helix periodicity of about 25–35 nm (Fig. 4J,K). These inclusions probably represent the intermediate form between intracellular and extracellular NFT. The Fig. 4I (small magnification) and 4L (large magnification) show autophagic vacuoles (AV) closely associated with paired helical fibrils in tryptamine-treated cells. These AV resemble neuronal AV of scrapie and Creutzfeldt-Jacob disease (Liberski et al., 1992). The distribution of TrpRS in tryptamine-treated cells was analyzed electron-microscopically using immunogold or peroxidase–antiperoxidase for detection of immunoreactivity. In tryptamine-treated cells immunostained with characterized polyclonal antibodies to TrpRS (Paley et al., 2006), the gold-associated immunoreactivity is localized preferably in association with NFT compared with the surrounding cytoplasm area (Fig. 5A). The TrpRS-positive NFTs made up of PHF (Fig. 5A, inset). The TrpRS-immunogold reactivity is revealed also in association with manifestations resembling AV (Fig. 5B). This vacuole represents a cytoplasm surrounded by twisted fibrils

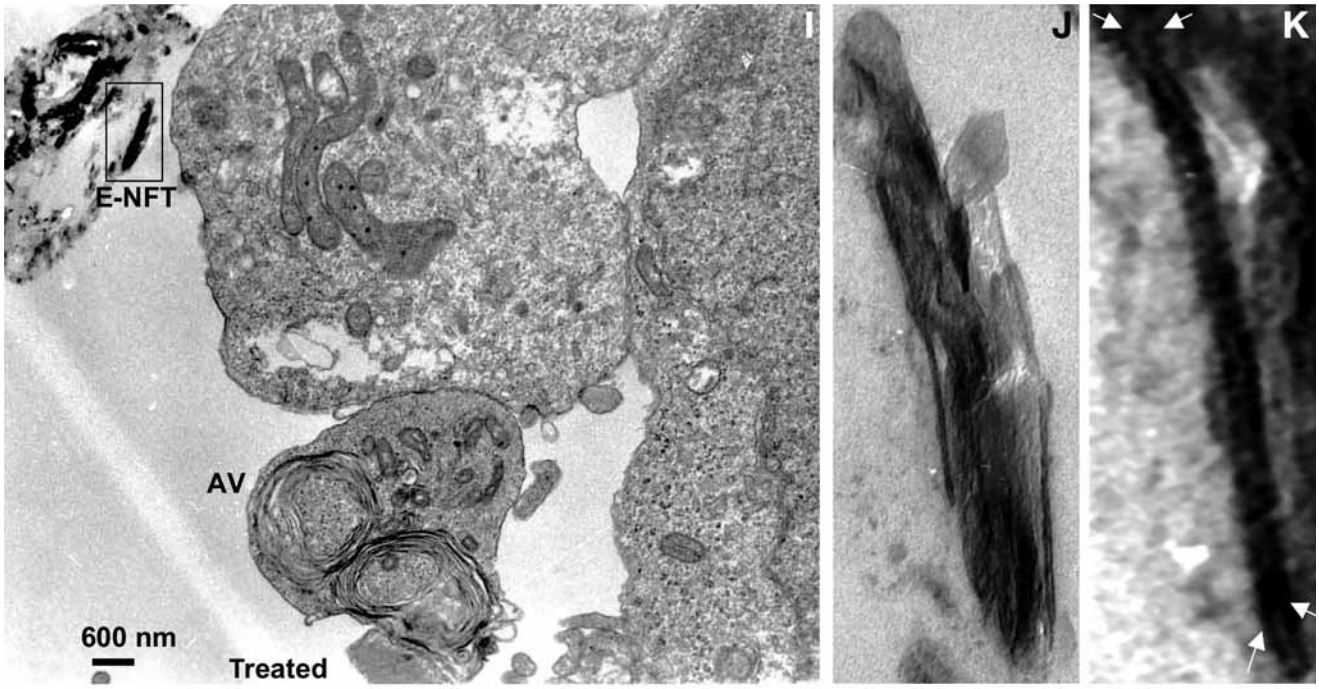

Fig. 4. *(Continued)*

with a diameter of about 10 nm (Fig. 5B, enlarged fragment). These fibrils seem to be made up of both membranous and filamentous materials. The TrpRS immunoreactivity was found inside the mitochondria containing AV (Fig. 5C). Using peroxidase–antiperoxidase technique intense TrpRS immunoreactivity was detected in intracellular (Fig. 5F–I), extracellular (Fig. 5E) and transitional between intracellular and extracellular manifestations (Fig. 5D) in tryptamine-treated cells. The high-magnification visualizes numerous twisted alkaline-resistant fibrils (Fig. 5I). The TrpRS presence in fibrillar deposits is likely a result of a self-assembly of TrpRS and its fragments in fibrils that we have previously demonstrated (Paley et al., 2006). We set out herein to confirm whether or not TrpRS-derived synthetic *N*-peptide self-assembles in paired helical fibrils. The Fig. 5K shows concentric (b) and linear (c) double-helical fibrils (d) self-assembled (a) by *N*-terminal TrpRS-derived synthetic peptide. This peptide lies within a TrpRS N-terminal extension domain proteolized in vivo.

Electron microscopy visualized the p-tau-AT8 MAb immunoreactivity associated with intracellular filamentous inclusion in tryptamine-treated cells (Fig. 5J). The inset with high magnification shows helical fibrils of about 10 nm in diameter in the paired segment (Fig. 5J). No immunoreactivity was detected in the cells following incubation with only secondary gold-conjugated antibodies or PAP (data not shown). The cells stained by anti-TrpRS antibodies depleted with excess of purified recombinant hTrpRS (Paley et al., 2006) showed no immunoreactivity (data not shown). Taken together the data indicate that (a) tryptamine is toxic for human neuronal cells at the concentrations inhibiting TrpRS, (b) tryptamine is more toxic for fast dividing neuroblasts than for slow dividing epithelial-like cells, (c) tryptamine induces formation of tangles of twisted fibrils, (d) TrpRS is accumulated in detergent-insoluble fraction and decreased in cytoplasm of tryptamine-treated cells, (e) TrpRS is detected in association with twisted fibrils in tryptamine-treated cells, and (f) TrpRS-derived synthetic peptide self-assembles in paired helical fibrils in vitro.

Histochemistry of Brain Sections

To extend the study of tryptamine effect on neuronal cells to in vivo level, the brains isolated from

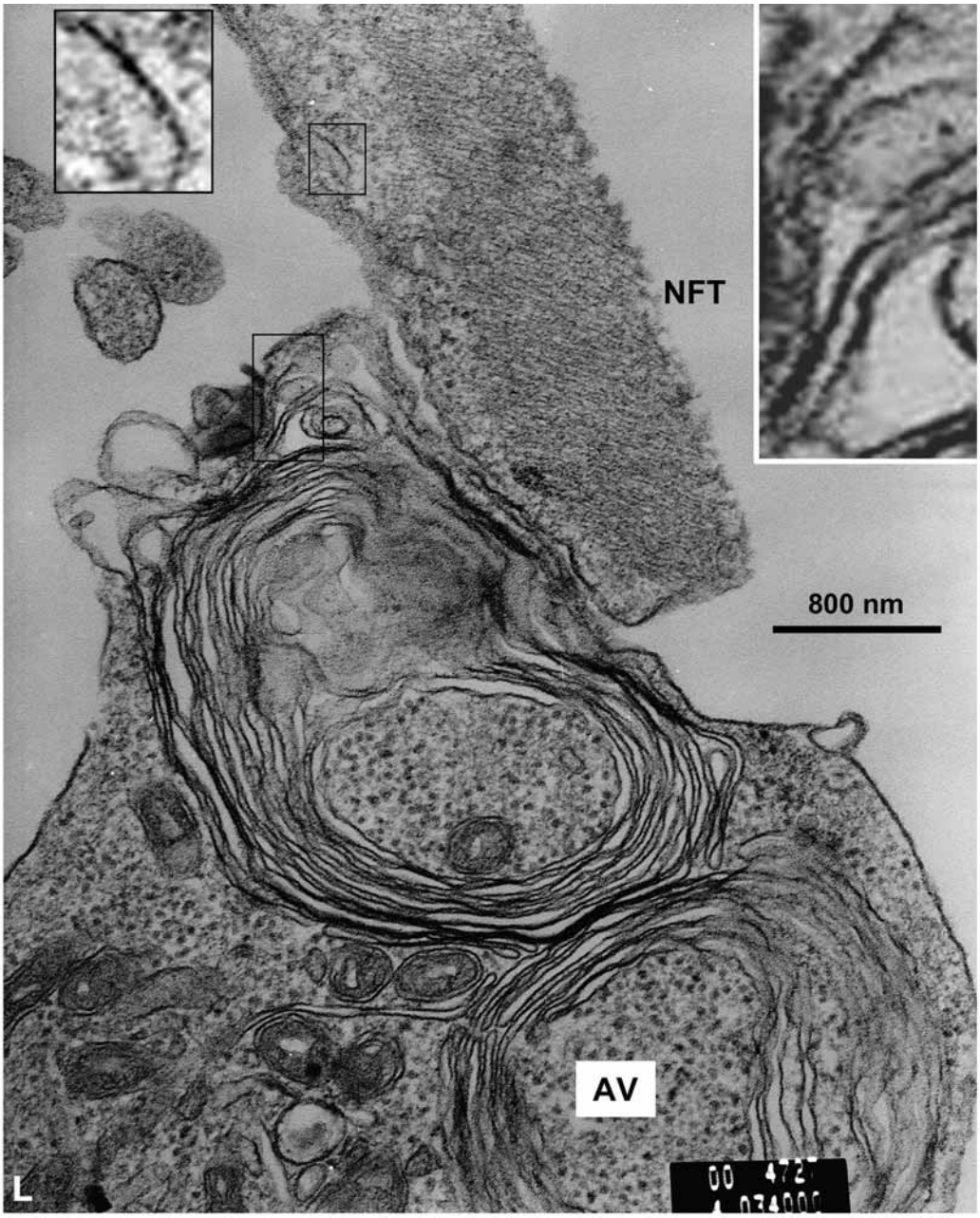

Fig. 4. Electron microscopy of control and tryptamine-treated cells. **(A,B)** Electron microscopy of untreated SH-SY5Y cells. B is a high-power photomicrograph of the area in A showing closely the absence of neurofibrillary degeneration. **(C–L)** Electron microscopy of tryptamine-treated cells. **(C–F)** NFT in different tryptamine-treated cells. The right panel of E is a high magnification of the area on E shown by arrow. **(G,H)** High magnification of areas framed in F. M, mitochondria; ER, endoplasmic reticulum. **(I)** Electron microscopy of cells with autopagic vacuoles and extracellular NFT bundles of fibrils. **(J,K)** High magnification of the area boxed in I. The white arrows show two fibrils at the termini of paired helical fibril. **(L)** High magnification of autopagic vacuoles visualized in Fig. 4I. Two insets on L are high-magnification images showing paired helical fibrils of the framed areas. Note the cells were treated with 20 μg/mL of tryptamine for 6 d.

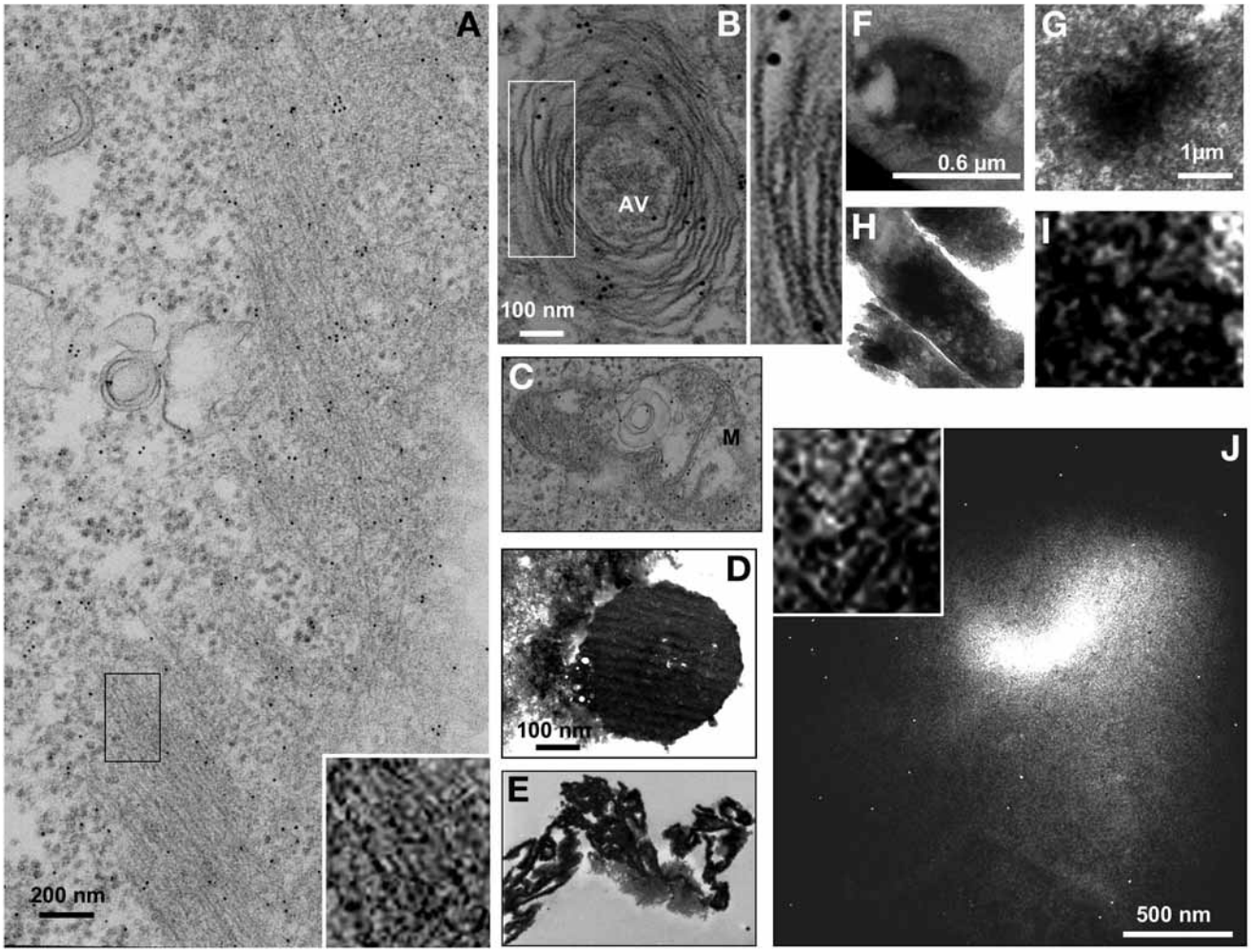

Fig. 5. *(Continued)*

the control and tryptamine-treated mice were histochemically analyzed. The brain sections were stained with Congo red that detects amyloid plaques and silver stained using Gallyas procedure that specifically detects NFT. The Fig. 6A shows significant difference between control and tryptamine-treated brains in histochemical staining. In contrast to the histochemical slides of control brains showing no reactivity with Congo red and Gallyas silver, the brain sections from tryptamine-treated mice are intensely stained by Gallyas and congophilic (Fig. 6A). The representative light microscope micrographs of sagittal brain sections reveal Congo red staining and birefringence of extracellular plaques in CA2-CA1 hippocampal area of tryptamine-treated mice, whereas a control hippocampus showed only hematoxylin counterstaining and no congophilia (Fig. 6B). Figure 6C visualizes amyloidosis, Congo red positive neurons and Gallyas silver-stained intracellular (white arrow) and extracellular (inset, black arrow) NFTs in cerebral cortex of tryptamine-treated mice. No such pathology was detected in the control mouse brain. The right image of tryptamine-treated cells shows high magnification of Gallyas-stained neurons and glia (Fig. 6C). Thus histochemical analysis demonstrates extracellular congophilic plaques with birefringence in hippocampus, congophilia, glial Gallyas silver staining, and intra- and extracellular NFT in cerebral cortex of tryptamine-treated mice.

Electron Microscopy of Mouse Hippocampus

The transmission electron microscopy of hippocampal sections from brains of control and tryptamine-treated mice is shown in Fig. 7. The neuron

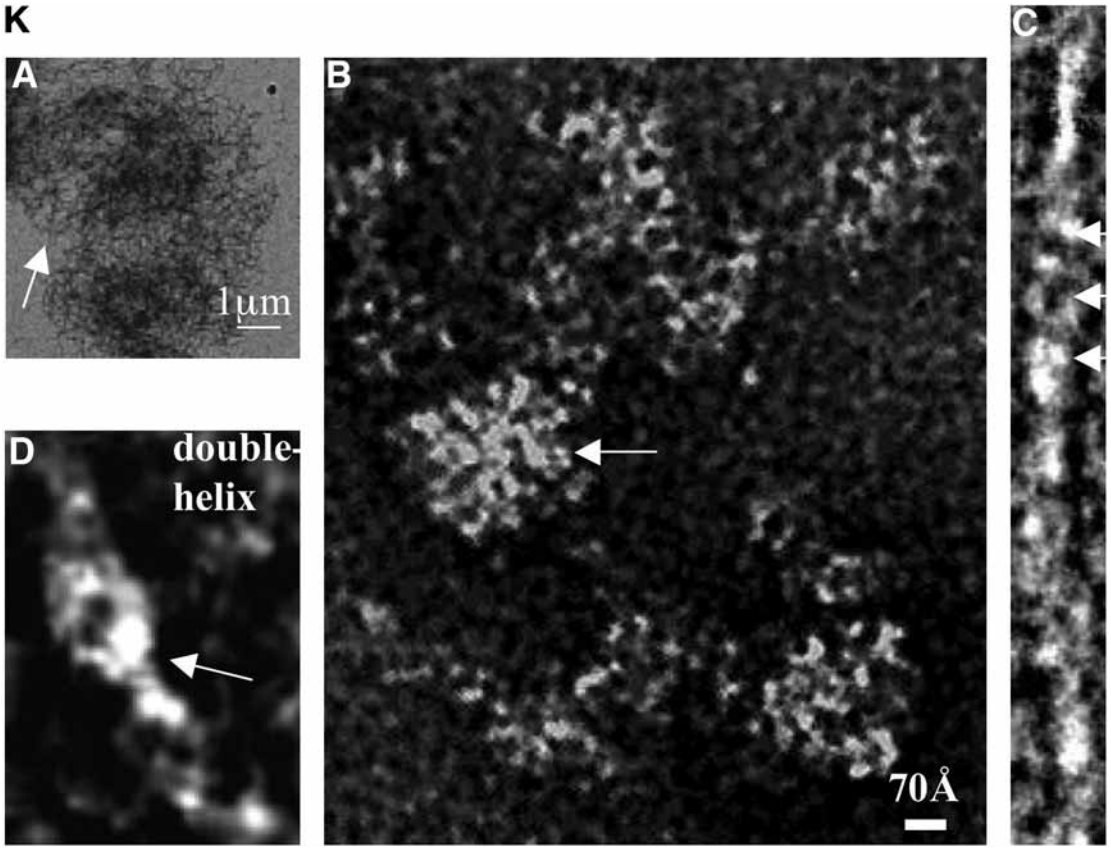

Fig. 5. Electron microscopy demonstrates association of TrpRS and p-tau with fribrils. **(A)** Immunoelectron microscopy of TrpRS immunogold reactivity in tryptamine-treated cells. Inset is a high magnification of the boxed area showing bundle of twisted fibrils. **(B)** Immunogold TrpRS reactivity associated with autophagic vacuole in tryptamine-treated cell. The right fragment is a high magnification of the area boxed in B showing twisted fibrils apparently associated with membranes of autophagic vacuoles. **(C)** Immunogold TrpRS reactivity in mitochondria (M) with vacuole. **(D–H)** Manifestations of different morphology are intensely immunostained with anti-TrpRS–PAP in tryptamine-treated cells. **(D)** Intracellular fibrils located within a cell periphery are associated with plaque-like formation that is partially located in the extracellular space. **(E)** Exracellular TrpRS-immunoreactive manifestation. **(F,G)** Intracellular fibrillar manifestations of different morphology. **(H)** Intense intracellular TrpRS immunoreactivity. **(I)** A high magnification of the area in H. **(J)** Immuno-electron microscopy of tryptamine-treated cell with p-tau AT8 immunogold reactivity associated with intracellular filamentous inclusion. The inset shows high magnification of paired helical filaments of the area in J. Note the cells were treated with 20 μg/mL for 6 d. **(K)** Electron microscopy of self-assembled TrpRS N-peptide. (a–d) A high-magnification of concentric (b) and double-helical fibrils (c and d) shown in a (small magnification).

with NFT in the pericarya is surrounded by twisted fibrils in the tryptamine-treated brain (Fig. 7A). The images B–D demonstrate high magnification of fibrils framed on Fig. 7A. Figure 7E,F, and I show three other neurons (N) with NFTs in pericarya. The Fig. 7H visualizes a glial cell with a nucleus (G) surrounded by twisted fibrils ranging from 25 to 35 nm in diameter. The glial fibrillary tangles were described earlier in the brains of patients with progressive supranuclear palsy (Nishimura et al., 1992). In the Fig. 7I, both neuron (N) and glia (G) located close to each other include helical fibrils (*see* insets) in pericarya. The neuronal helical fibrils, which are measured to be about 10–26 nm in diameter with a helix periodicity of about 70–118 nm are close to PHF sizes of the NFT in AD brain (Tabaton et al., 1991). No NFT have been detected in neurons and glia of hippocampus from the control mice (Fig. 7J).

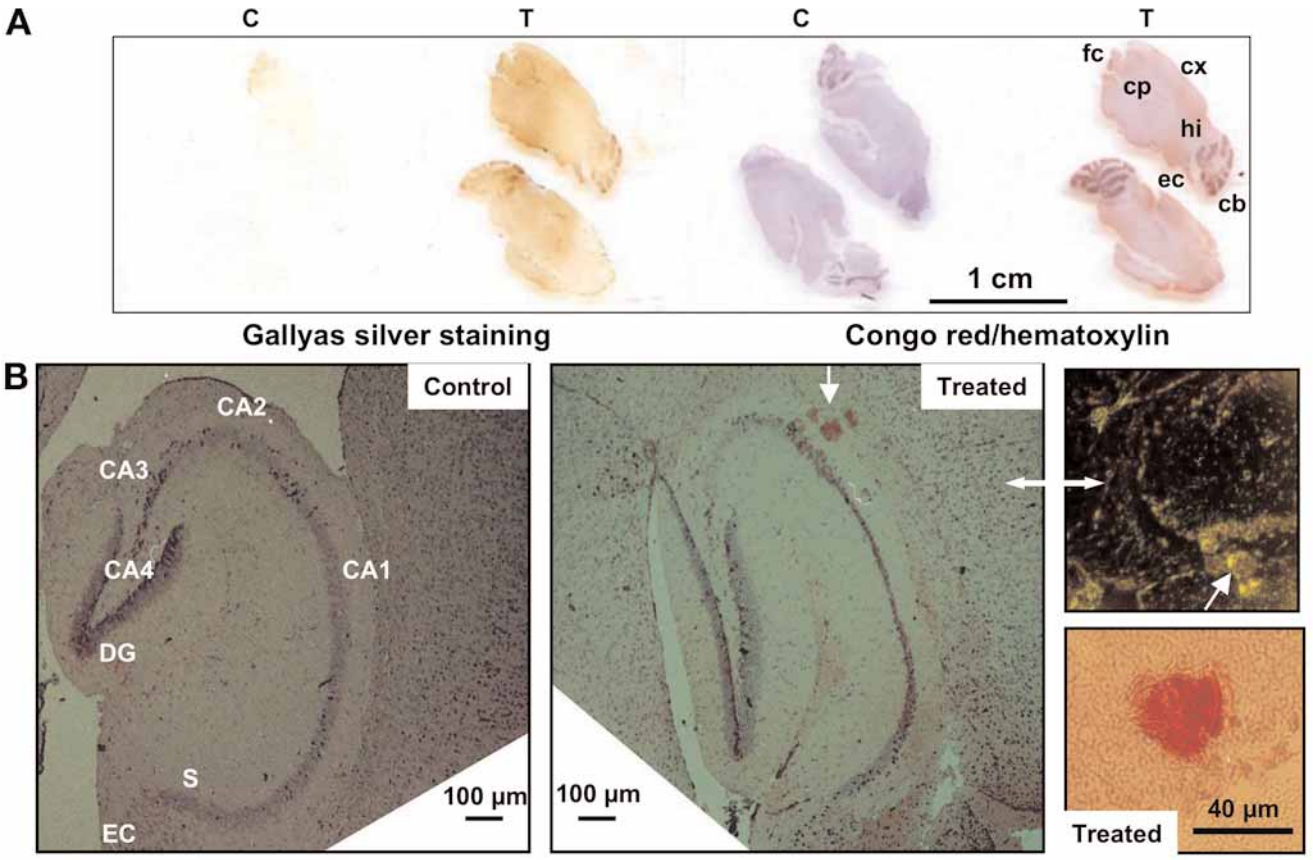

Fig. 6. *(Continued)*

Neurons Counting

The histochemical staining shown above on Fig. 6B visualizes apparent decrease in staining of certain hippocampal areas from tryptamine-treated mice compared with control mice. Here the Fig. 8 shows representative enlarged micrographs of hematoxylin stained hippocampal areas CA1 (Fig. 8A–D), DG (Fig. 8E–H), and CA3–4 (Fig. 8I,J) of tryptamine-treated and control mice. The manual counting of neurons was conducted as described in materials and methods and included three hippocampal areas: CA1, DG, and CA3–4. The number of hematoxylin stained neurons was significantly reduced in tryptamine-treated group compared with control group about 60% in CA1 area, about 90% in DG and about 40% in CA3–4 area ($p < 0.05\%$). This decrease is an indicator of a significant neuronal loss in the specific hippocampal areas. No attempt was intended to quantify a total number of neurons in brain of mice.

Behavior of Mice

To analyze the effect of tryptamine on mice behavior, the experiments with stick were designed. Different conditions were examined, i.e., stick was maintained on the heights of 12, 30, and 70 cm above the platform. It was found that 30 cm is the optimal height. The time of halting and running as well as the distance that was completed without falls were measured. The representative data of four experiments at different trial days are shown in the Table 1. A significant difference was observed in a behavior on the stick between control and treated mice following 4 mo of injections at a doze 50 μg per mouse per week. Specifically, seven of nine control mice completed the way and the only one mouse was halting at the start, whereas, all 10 examined tryptamine mice were halting at the start and no one completed the way. The seven of ten treated mice had never initiated movement. Following 3-mo treatment, the

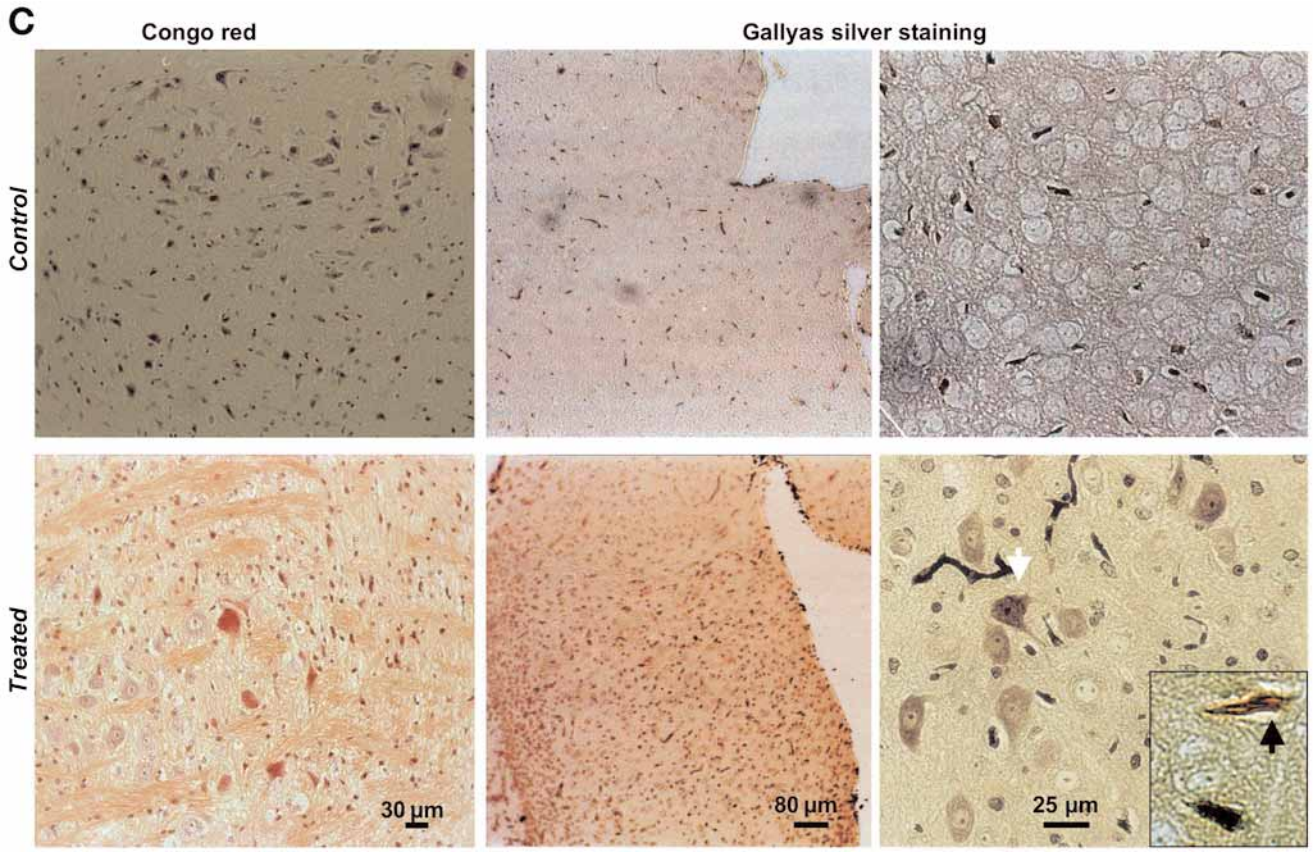

Fig. 6. Histochemistry of brain from control and tryptamine-treated mice. **(A)** Scan of Congo red and Gallyas silver-stained slides with the sagittal brain sections of control (C) and tryptamine-treated (T) mice. Marks on slides are: cb, cerebellum; cx, cortex; hi, hippocampus; cp, caudate putamen; ec, entorhinal cortex; and fc, frontal cortex. **(B)** Light microscopy of Congo red/hematoxylin staining of hippocampal areas from control and tryptamine-treated mice. The white arrows point congophilic compact plaques in CA2-CA1 hippocampal area and a birefringence of the same area (right panel). Lower right panel visualizes fibrillar congophilic plaque in hippocampus of tryptamine mouse. **(C)** Light microscopy of Congo red/hematoxylin and Gallyas silver staining of neurons in the cerebral cortex of control and tryptamine-treated mice. Central panels show a low magnification, and right panels show a higher magnification of the same area. White arrow indicates intracellular NFT and black arrow on inset indicates extracellular NFT.

essential difference between control and treated mice was also detected in behavior on stick located 12 and 70 cm above the platform (data not shown). It is known from different sources that later signs of AD are visibly impaired movement or coordination, including slowing of movements, halting gait and reduced sense of balance, frequent falls, problems with motor function: twitching and spasm (commonly as early-onset in familial cases), tendency to have seizure (Weiner et al., 2003). These symptoms were observed after treatment with tryptamine at different dozes. On the other side, the normal aging is also characterized by increasing caution in movement and slower reaction times. The effect of tryptamine on the mouse behavior was then examined in swimming experiments. In the present swimming experiments no attempt was intended to examine effect of tryptamine on learning performance because in the pretraining swimming exercises both control and tryptamine-treated mice were continuously fatigued. The fatigue visibly increased escape latency between the first and the third sessions. As was earlier shown a physical fatigue effects a learning performance of Balb/c mice in the Morris water

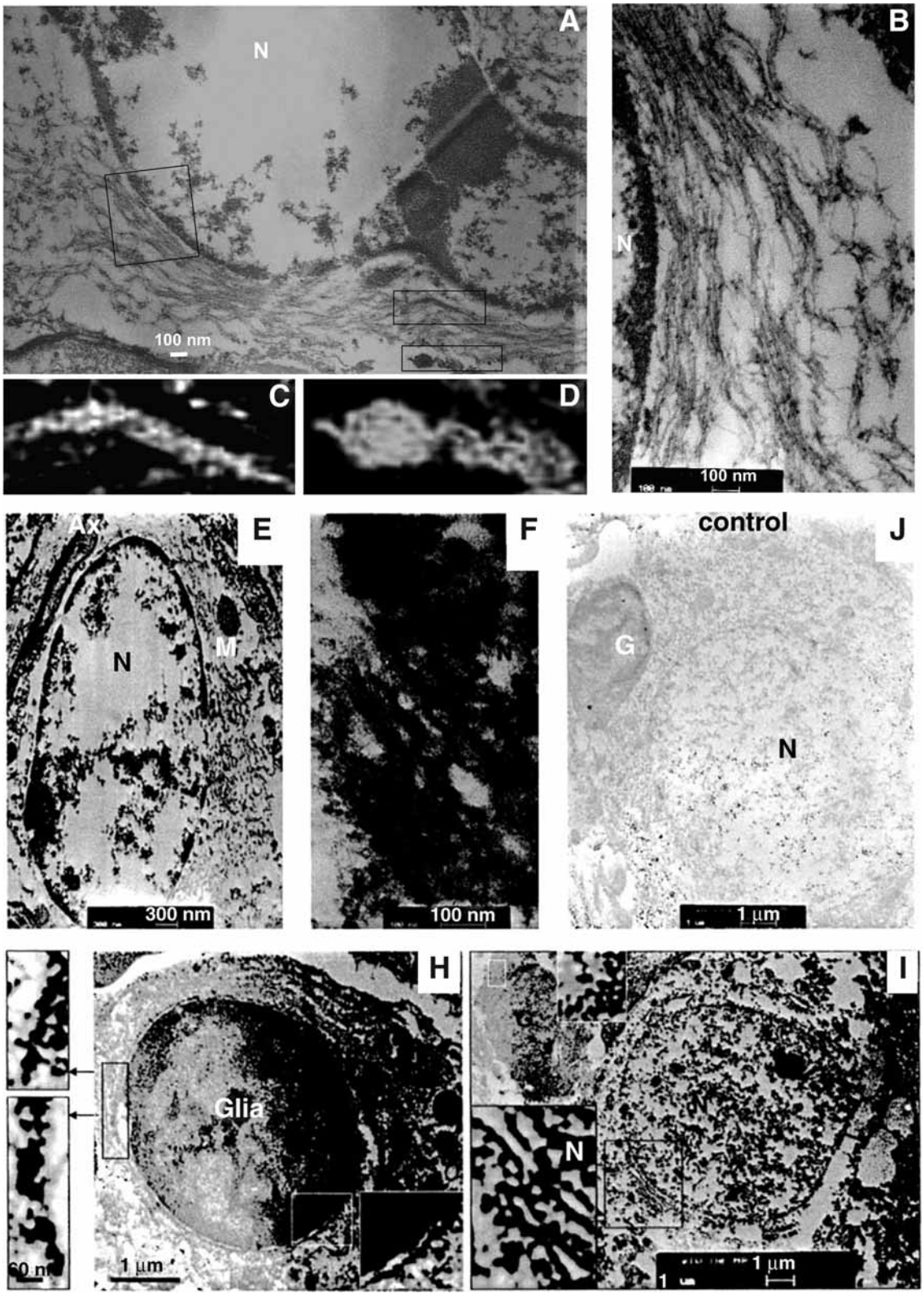
A
N
100 nm
B
N
100 nm
C
D
Ax
E
N
M
300 nm
F
100 nm
control
J
G
N
1 µm
H
Glia
1 µm
I
N
1 µm

Table 1
Behavior of Mice on Stick

Control, time (s)			Tryptamine, time (s)		
Halt	Run	Way (%)	Halt	Run	Way (%)
0	33	100	50	2	40
0	22	100	47	0	0
0	53	50	11	0	0
20	0	10	17	0	0
0	22	100	40	10	20
0	20	100	3	17	50
0	17	10	9	0	0
0	15	100	3	0	0
0	16	100	15	0	0

Mice were examined following 4 mo of treatment with tryptamine at 50 µg per mouse once per week or placebo. Stick of 80 cm was located 30 cm above the plateau. Time of halting and running on the stick was measured in seconds.

maze (Mizunoya et al., 2004). Herein we analyzed effect of tryptamine on escape latency between the first and the third sessions. In 33% of swimming exercises of control mice and 66% of tryptamine-treated mice the speed in finding hidden platform in 90-cm pool was reduced between the first and the second sessions of the same trial day with maximum decrease of 9.6 times for control mice and 20 times for treated mice. These values are reproducible in repeated trials of different trial days. The speed between the second and the third sessions in the same trial was reduced by 66% for control mice with maximum reduction 5.7 times and by 72% for the tryptamine mice with maximum reduction four times. In the smaller swimming pool of 50 cm in diameter the control mice tried to escape from the pool, whereas, tryptamine-treated mice did not show the motivation to escape. Thus tryptamine treatment led to significant increase in escape latency between the first and the second swimming sessions compared with the control group. No significant difference in swimming speed to find a hidden platform by control and treated groups was observed between the second and the third sessions likely because of the fatigue of the control mice. The tryptamine-induced reduction in speed can be result of increased fatigue and also impaired locomotor activity.

PET Brain Imaging and Blood Glucose

Measurement of local cerebral glucose metabolism by PET with ^{18}F-FDG has become a standard technique. Many studies have documented a close relation between cerebral glucose metabolism and cognitive functions (Perani et al., 1993). In the authors' study, tryptamine treatment led to decrease in the level of blood glucose by 6.5% compared with the control. Meanwhile, the tryptamine-treated animals gained more weight than the control animals. Starting from the weight of 24.2 ± 0.9 g, the weight progression was 20.8 ± 3.8% in tryptamine-treated animals, while the increase in the control group was 11.4 ± 4.5% (Table 2). The PET studies of glucose utilization revealed local decreases in glucose utilization, whereas the average whole brain glucose utilization did not change. Highest decrease was observed in hippocampus, the average decrease being 5.6% compared with the control group (Table 2; Fig. 9). The increase of weight that we observed in the treated mice might be result of hyperphagia, which was described for AD (Smith et al., 1998). The authors' data on tryptamine-induced decrease in the level of blood glucose might by attributed to hyperinsulinemia, which was shown to be induced by tryptamine (Sugimoto et al., 1991) and is also observed in AD (Carantoni et al., 2000). Not being a definite diagnostic tool for AD, the PET-imaging with 18-FDG has been successfully used for AD diagnosis especially based on reduced glucose metabolism in hippocampus (De Santi et al., 2001).

Fig. 7. *(Opposite page)* Electron microscopy of hippocampus from control and tryptamine-treated mice. **(A)** EM of neuronal nucleus (N) surrounded with twisted filaments in tryptamine-treated brain. **(B–D)** High magnification of the areas boxed in A. **(E,F,I)** The three different hyppocampal neurons and glia cell (I) with twisted fibrils in perikarya. Insets on I show high magnification of helical filaments surrounding neuronal (N) and glial (G) nuclei. **(H)** Glia cell with twisted fibrils surrounding nucleus. Inset shows a high magnification of the boxed area in H. Two left panels show a high magnification of the area framed in H and shown with arrows. **(J)** Hippocampal neuron and glia of the control mouse. N, nucleus of neuron; G, nucleus of glia; M, mitochondria; Ax, axon.

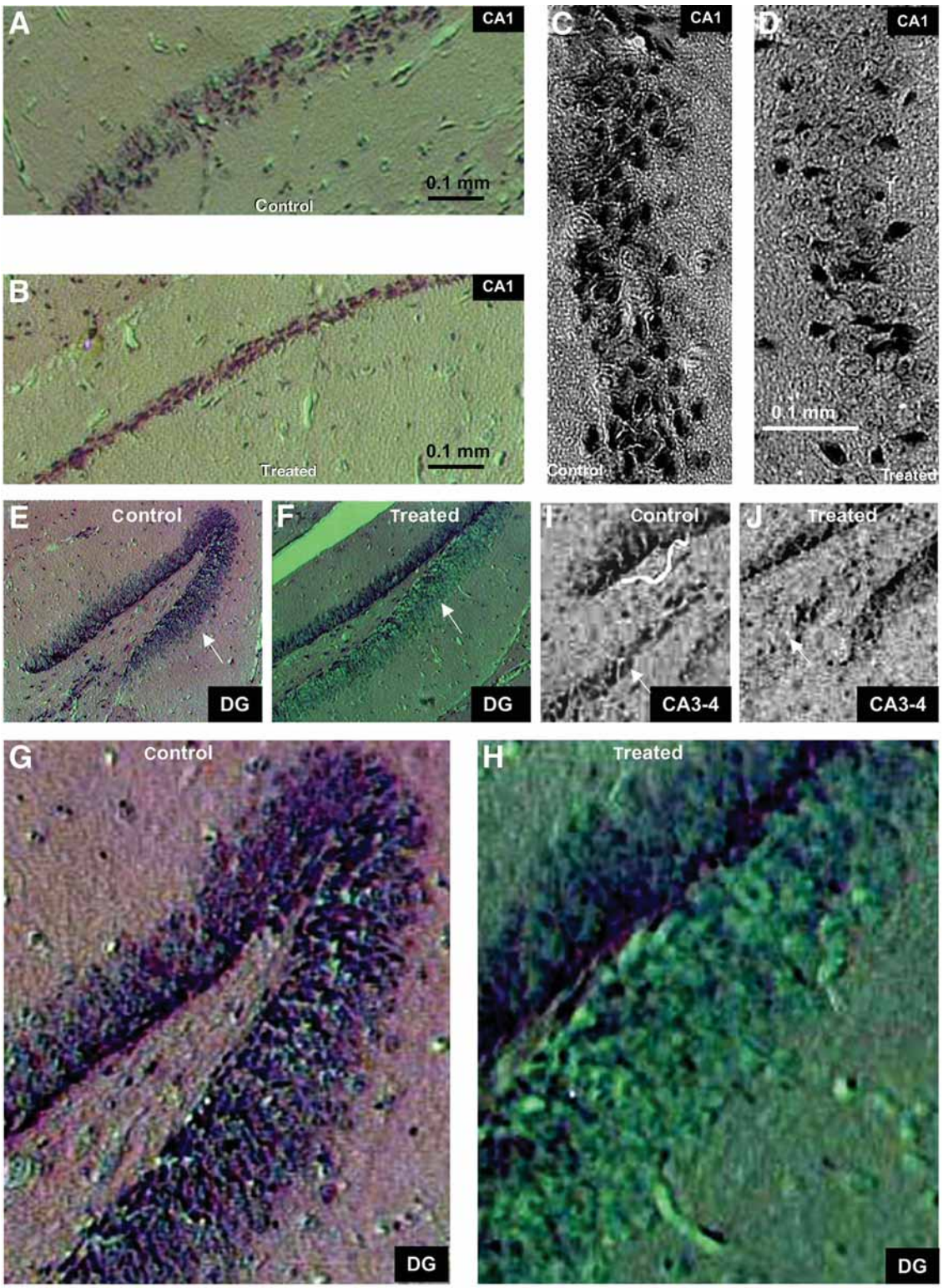
A
CA1
0.1 mm
Control
B
CA1
0.1 mm
Treated
C
CA1
Control
D
CA1
0.1 mm
Treated
E
Control
DG
F
Treated
DG
I
Control
CA3-4
J
Treated
CA3-4
G
Control
DG
H
Treated
DG

Dependence of tRNA Aminoacylation on Concentrations of Amino Acids

To analyze weather or not tryptophan at increasing concentrations can enhance the hTrpRS aminoacylation and consequently compensate the tryptamine inhibitory effect, we have analyzed a concentration dependence of an essential amino acid, tryptophan, which is a least available amino acid in food and a concentration dependence of glutamic acid, a nonessential and the most available amino acid in food in the reaction of tRNA aminoacylation using extract from human SH-SY5Y neuroblast cells as a source of aminoacyl-tRNA synthetases. Significant difference between optimal concentrations for tryptophan and glutamic acid in tRNA aminoacylation reactions (Fig. 10) were found. Surprisingly, tryptophan at the concentration 50 μ*M* inhibits TrpRS by 85%, whereas glutamic acid even at 500 μ*M* increases GluRS activity (Fig. 10). The reaction reached maximum at 10 μ*M* tryptophan, whereas 500 μ*M* tryptophan led to 100% TrpRS inhibition. Normally, an increase in substrate concentration increases the velocity of the enzyme reaction. Some enzymes, however, display the phenomenon of excess substrate inhibition (Bardsley et al., 1983). In other words, the large amounts of substrate can have the opposite effect and actually slow down the reaction. The present data indicate that tryptophan concentration is critical for protein biosynthesis and increase in tryptophan consumption might not compensate a possible tryptamine inhibitory effect.

Table 2
Blood-Glucose Level, Weight Progression, and Positron Emission Tomography Studies of Glucose Utilization

Control animals	Tryptamine-treated	
Blood glucose (mg/dL)	138 ± 19	129 ± 19
Weight progression (%)	11.4 ± 4.5	20.8±3.8 (63 d)
Glucose utilization (standardized unit values)		
Whole brain	0.94 ± 0.11	0.95 ± 0.18
Cerebellum	0.72 ± 0.12	0.68 ± 0.07
Cingulate	1.29 ± 0.10	1.27 ± 0.13
Hippocampus	1.24 ± 0.11	1.17 ± 0.17
Olfactory area	1.43 ± 0.21	1.36 ± 0.13
Striatum	1.21 ± 0.12	1.17 ± 0.16

The control mice injected with PBS and tryptamine-treated mice were examined.

Discussion

NFT and Neuronal Loss

In this study, the authors have developed procedures for tryptamine treatment of human neuronal cells and mice using range of dozes that enabled to inhibit TrpRS enzymatic activity. The authors have showed here that neuroblastic and epithelial-like neuronal cells express distinctive sensitivity to tryptamine inhibitory effect have been shown here. Previously, this had been demonstrated that levels of TrpRS in kidney-cultured cells varied from cell to cell of the same cell line (Paley et al., 1991). Moreover, the mammalian TrpRS levels in each organ varied from animal to animal of the same species (Favorova et al., 1989). Thus, the degree of tryptamine inhibition might also vary from cell to cell. In our attempts to develop a relevant model of neurodegeneration, the variations in TrpRS level were considered. Therefore, we used varying dozes of tryptamine to reach the saturating concentrations that would inhibit TrpRS, damage-selected cells but would keep the animal alive and in good physical conditions. As soon as the effect of tryptamine is dose-dependent and time-dependent, it might lead to mild, moderate, or severe degeneration depending on a level of inhibition and subsequently percent of a cell loss resulting from the treatment. We suggest that elevation of tryptamine in any sensitive cells can lead eventually to their degeneration. Here, we have characterized nontransgenic tryptamine-induced human cell and mouse models of neurodegeneration-expressing NFT made up of twisted fibrils. The pathological manifestations associated with NFT are reported

Fig. 8. *(Opposite page)* Hematoxylin staining of hippocampal areas from sagittal sections of brain from control and tryptamine treated mice. **(A–D)** CA1 hippocampal area. **(C,D)** Enlarged images of A and B. **(E–H)** Dentate girus (DG) area of hippocampus. **(G,H)** Enlarged images of E and F. **(I,J)** CA3–4 areas of hippocampus.

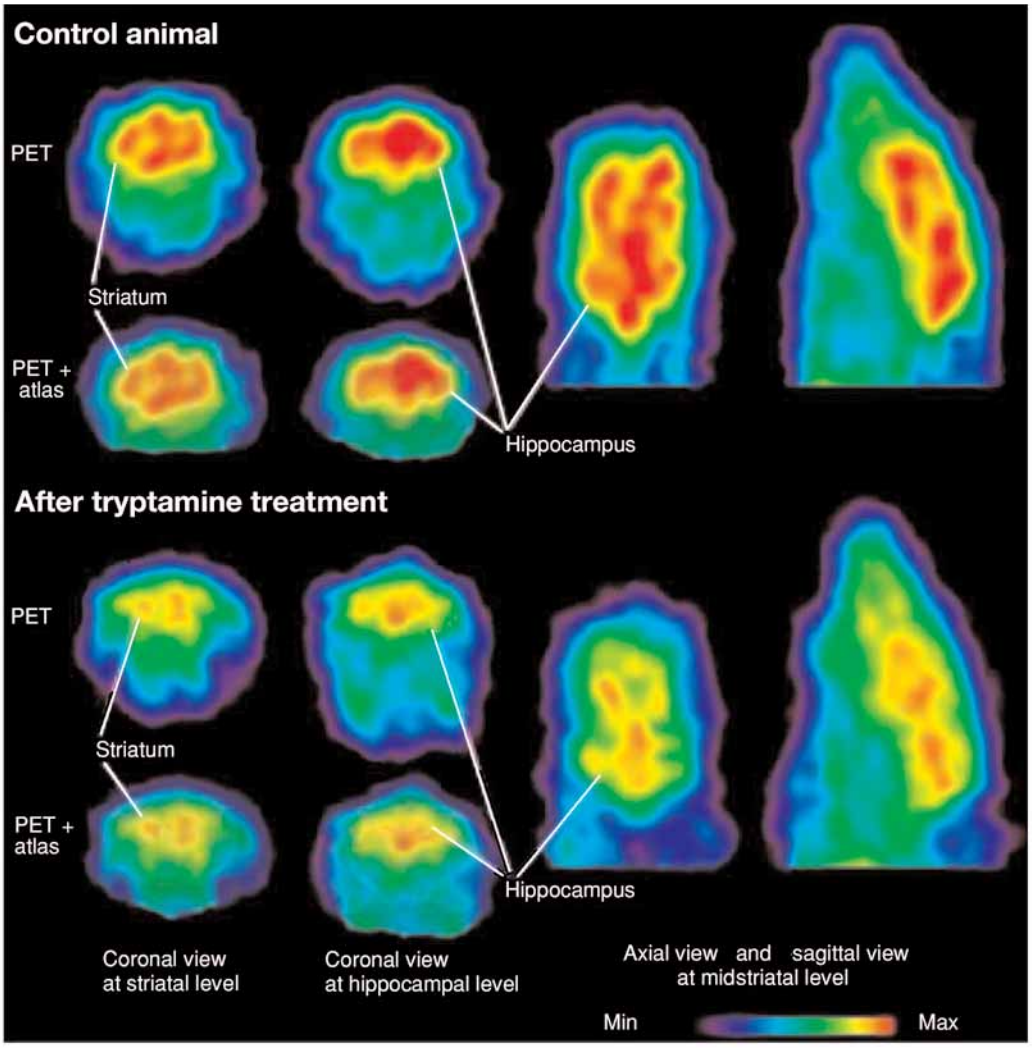

Fig. 9. Color-coded positron emission tomography images of the accumulation of ^{18}F-FDG in a control and tryptamine-treated mouse brain. Coronal slices show the activity distribution at the midstriatal and midhippocampal levels at the time-point 40–45 min after administration of the radioactivity. Axial and sagittal views show ^{18}F-FDG accumulation at the midstriatal level. To demonstrate localization of ^{18}F-FDG distribution, the coronal slices were overlaid with anatomical borderlines obtained from a mouse atlas.

in brain of patients with a number of progressive neurodegenerative diseases, including AD, PD, Creutzfeldt-Jacob's disease, Gerstmann–Straussler–Scheinker's disease, scrapie, rabies, Down syndrome, forms of frontotemporal dementia, Pick's disease, corticobasal degeneration, and progressive supranuclear palsy (Spillantini and Goedert, 1998). The fibrillary tangles of paired and straight filaments that closely resemble NFT were found in other tissues of AD, such as kidney, pancreas, liver, thyroid, prostate, and ovary (Miklossy et al., 1999). It was estimated that the NFT, but not senile plaques are parallel to the duration and severity of AD (Arriagada et al., 1992), whereas neuronal loss parallels but exceeds NFT formation (Gomez-Isla et al., 1997). However, the mechanism of NFT formation is not clearly understood and the agent that leads to this formation is unidentified. Despite the fact that only about 2–10% of AD cases are associated with different genetic mutations, the nontransgenic models have not yet been reported. The transgenic models that express neurofibrillary

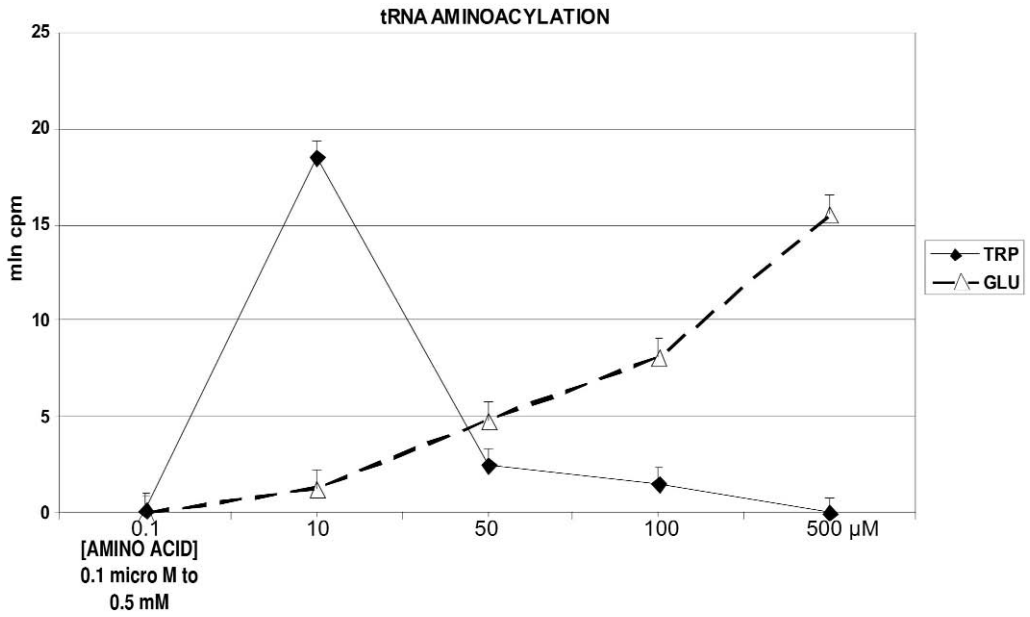

Fig. 10. Dependence of $tRNA^{trp}$ aminoacylation on amino acid concentrations. The aminoacylation of mammalian tRNA with L-tryptophan and L-glutamic acid was catalyzed by aminoacyl-tRNA synthetases from SH-SY5Y human neuroblast cell extract.

pathology in brain are constructed by using mutated gene for tau protein on chromosome 17 (Gotz et al., 2004). This gene was not found to be mutated in AD (Spillantini and Goedert, 1998) but is mutated in the minority of cases with frontotemporal demenia (Levchenko et al., 2004). The cause of sporadic AD is still unknown (Gotz et al., 2004). The tryptamine-induced cell and animal models with both neuronal loss and NFT might explain the cause of diseases associated with degeneration and loss of selected cells. The neuronal loss in hippocampal CA1 area that was revealed in tryptamine-treated mice is also associated with AD (von Gunten et al., 2006).

Tryptamine

Tryptamine possesses plural physiological dose-dependent effects. Tryptamine is a neuromodulator with apparent mainly excitant behavioral effects, but a loss of locomotor activity and catatonia with tremor and rigidity were also observed (Mousseau, 1993). Additionally, tryptamine increases glucose transport (Fischer et al., 1995) induces hyperinsulinemia and hypoglycemia (Sugimoto et al., 1991), hyperglucagonemia (Sugimoto et al., 1994), hypertension (Jacob and Michaud, 1962), decreases the digital arterial blood flow (Bailey et al., 2004), has anorexic effect (Fletcher and Paterson, 1989), DNA-binding activity (Helene et al., 1971), mitogenic activity (Nemecek et al., 1986), mutagenic or antimutagenic dose-dependent effects (Abu-Shakra, 1992), induces hypothermia (Yamada et al., 1987b) or hyperthermia (Cox et al., 1981), seizures at 20 mg/kg (Okuyama et al., 1997), and impairs the reproduction in *Drosophila melanogaster* (Thomas et al., 1998). Tryptamine iv was administered in a dose greater than 15 mg/kg induced distinct head-weaving and hindlimb abduction in mice (Yamada et al., 1987a). Tryptamine, applied to cortical neurons, had depressant effects (Jones, 1982). In the earlier reports tryptamine was shown to be cytotoxic for mammalian and human cells (Paley et al., 1991; Paley, 1999). Tryptamine might affect the behavior as a precursor of methyltryptamines. Dimethyltryptamine is a natural product of tryptamine methabolism. Dimethyltryptamine is a psychedelic–hallucinogen found in plants, animals, fungi, and frog (Forsstrom et al., 2001). Tryptamine itself is not a hallucinogen, but hallucinations might be associated with conversion of the elevated tryptamine to its methylated analogs at a higher rate that it occurs normally.

Note some AD disease symptoms are hallucinations or delusions (Weiner et al., 2003). However, most of the evidence regarding the involvement of tryptamine in neuropsychiatric syndromes is indirect given its postmortem instability and the lack of sensitivity of most of the earlier methods of detection (Mousseau and Butterworth, 1995).

Tryptamine to Tryptophan Ratio

Tryptamine is an inhibitor that competes with tryptophan for binding to TrpRS active site (Kisselev et al., 1979; Fromant et al., 1981; Lowe and Tansley, 1984). Tryptamine at the concentration 1.6 m*M* leads to 50% reduction of the initial rate of tryptophan-dependent [$^{32}PP_i$]-ATP exchange reaction catalyzed by *E. coli* TrpRS in the presence of 2 m*M* tryptophan (Fromant et al., 1981). Accordingly, to inhibit TrpRS the tryptamine concentration should not exceed a concentration of tryptophan. Tryptophan is known as a least available amino acid in food, but some foodstuffs contain no tryptophan, for example, Chinese noodles (soybean starch or potato + bean-starch) (Bremer et al., 1996). Consequently, the consumption of meal including foodstuffs with a low level or no tryptophan together with a food containing high concentrations of tryptamine might lead to an increase in the tryptamine to tryptophan ratio. The authors' present data (Fig. 10) show 85% substrate inhibition of human TrpRS by tryptophan at 50 μ*M*. The results on the tryptophan dependence with a maximum of aminoacylation reaction at about 10 μ*M* tryptophan (Fig. 10) are in a good agreement with a free tryptophan content at about 6 μ*M* in human plasma (Demling et al., 1996). Thus, the concentration of tryptophan in cells and a tryptamine/tryptopan ratio seem to be critical values for protein biosynthesis and cell survival.

Tryptophanyl-tRNA Synthetase

In this study, TrpRS is elevated in the detergent-insoluble cytoskeleton fraction and decreased in the cytosolic fraction of tryptamine-treated human neuronal cells. Moreover, in our immuno-electron microscopy data, about three times more TrpRS immunogold reactivity was associated with NFT than with the cytoplasm of tryptamine-treated human neuronal cells. In the authors' earlier study, the elevated TrpRS level was detected in the detergent-insoluble fraction of tryptamine-treated bovine kidney MDBK cells (Paley et al., 1991). It was shown that biochemically purified bovine TrpRS is very susceptible to aggregation (Tuzikov et al., 1991) and recombinant hTrpRS and TrpRS-derived synthetic peptides self-assemble in fibrils (Paley et al., 2006), specifically double-helical fibrils (Fig. 5K). Taken together, these data support that inactivated by tryptamine TrpRS might at least partially aggregate. The aggregated TrpRS would become detergent-insoluble similar to other aggregated proteins (Mimnaugh et al., 2004). This might lead to TrpRS decrease in soluble fraction and its increase in insoluble fraction. In other words, the increase of detergent-insoluble TrpRS might indicate that it was aggregated. Thus, tryptamine caused TrpRS redistribution from detergent-soluble to detergent-insoluble fraction. These observations support a mechanism whereby the tryptamine simultaneously inactivates TrpRS and promotes the accumulation of aggregated and potentially cytotoxic form of TrpRS. The significant cytotoxicity was shown for fibrils of TrpRS-N-terminal peptide (Paley et al., 2006). The protein aggregation leads to amyloid deposition, which is a key event in AD (Arriagada et al., 1992). In this study, Congo red staining revealed intense amyloidosis in cerebral neurons of tryptamine-treated mice similar to intraneuronal Congo red staining in AD brain (Rosenblum, 1999). It indicates that the protein aggregation has indeed occurred after the tryptamine treatment.

Acknowledgments

The authors thank Drs. John Q. Trojanowski and Pawel P. Liberski for reading manuscript and helpful comments. The authors thank Dr. Vera Shinder for help with electron microscopy of cells, Dr. Niko Grigorieff for help with electron microscopy of brain sections, and Dr. Aijun Zhu for help in PET imaging. This work was supported partially by fellowship from the Israel Gileadi's Program and Grants from the Israel Ministry of Health and the Israel Ministry of Science to E.L.P, fellowship from the Jane Coffin Childs Memorial Fund for Medical Research to O.S., and NIH/NIBIB grant EB01850 for A-L.B.

References

Abu-Shakra A. (1992) The modulatory effects of tryptamine and tyramine on the S9-mediated

mutagenesis of IQ and MeIQ in Salmonella strain TA98. *Teratog. Carcinog. Mutagen* **12,** 187–196.

Adeghate E. and Parvez H. (2004) The effect of diabetes mellitus on the morphology and physiology of monoamine oxidase in the pancreas. *Neurotoxicology* **25,** 167–173.

Anderson G. M., Gerner R. H., Cohen D. J., and Fairbanks L. (1984) Central tryptamine turnover in depression, schizophrenia, and anorexia: measurement of indoleacetic acid in cerebrospinal fluid. *Biol. Psychiatry* **19,** 1427–1435.

Arpi M., Vancanneyt M., Swings J., and Leisner J. J. (2003) Six cases of Lactobacillus bacteraemia: identification of organisms and antibiotic susceptibility and therapy. *Scand. J. Infect. Dis*. **35,** 404–408.

Arriagada P. V., Growdon J. H., Hedley-Whyte E. T., and Hyman B. T. (1992) Neurofibrillary tangles but not senile plaques parallel duration and severity of Alzheimer's disease. *Neurology* **42,** 631–639.

Badria F. A. (2002) Melatonin, serotonin, and tryptamine in some Egyptian food and medicinal plants. *J. Med. Food* **5,** 153–157.

Bailey S. R., Menzies-Gow N. J., Marr C. M., and Elliott J. (2004) The effects of vasoactive amines found in the equine hindgut on digital blood flow in the normal horse. *Equine Vet. J.* **36,** 267–372.

Bardsley W. G., Solano-Munoz F., Wright A. J., and McGinlay P. B. (1983*)* Inhibition of enzyme-catalysed reactions by excess substrate. A theoretical and Monte Carlo study of turning points in v(S) graphs. *J. Mol. Biol*. **169,** 597–617.

Biedler J., Helson L., and Spengler B. A. (1973) Morphology and growth, tumorigenicity, and cytogenetics of human neuroblastoma cells in continuous culture. *Cancer Res*. **33,** 2643–2652.

Bover-Cid S., Hugas M., Izquierdo-Pulido M., and Vidal-Carou M. C. (2001) Amino acid-decarboxylase activity of bacteria isolated from fermented pork sausages. *Int. J. Food Microbiol*. **66,** 185–189.

Bremer H. J., Anninos A., and Schultz B. (1996) Amino acid composition of food products used in the treatment of patients with disorders of the amino acid and protein metabolism. *Eur. J. Pediatr.* **155,** S108–S114.

Carantoni M., Zuliani G., Munari M. R., D'Elia K., Palmieri E., and Fellin R. (2000) Alzheimer disease and vascular dementia: relationships with fasting glucose and insulin levels. *Dement. Geriatr. Cogn. Disord.* **11,** 176–180.

Chanut E., Trouvin J. H., Bondoux D., Gardier A., Launay J. M., and Jacquot C. (1993) Metabolism of 6-fluoro-DL-tryptophan and its specific effects on the rat brain serotoninergic pathway. *Biochem. Pharmacol*. **45,** 1049–1057.

Cherin P. (1999) Treatment of inclusion body myositis. *Curr. Opin. Rheumatol*. **11,** 456–461.

Cox B., Lee T. F., and Martin D. (1981) Different hypothalamic receptors mediate 5-hydroxytryptamine- and tryptamine-induced core temperature changes in the rat. *Br. J. Pharmacol*. **72,** 477–482.

Davis P. K. and Johnson G. V. W. (1999) Energy metabolism and protein phosphorylation during apoptosis: a phosphorylation study of tau and high-molecular-weight tau in differentiated PC12 cells. *Biochem. J.* **340,** 51–58.

Demling J., Langer K., and Mehr M. Q. (1996) Age dependence of large neutral amino acid levels in plasma. Focus on Tryptophan, in *The Recent Advances in Tryptophan Research*, Filippini, G. A. ed., Plenum Press, New York, pp. 579–582.

De Santi S., de Leon M. J., Rusinek H., et al. (2001) Hippocampal formation glucose metabolism and volume losses in MCI and AD. *Neurobiol. Aging* **22,** 529–539.

Dewhurst W. G. (1968) New theory of cerebral amine function and its clinical application. *Nature* **218,** 1130–1133.

Domino E. F. and Gahagan S. (1977) In vitro half-life of 14-C-tryptamine in whole blood of drug-free chronic schizophrenic patients. *Am. J. Psychiatry* **134,** 1280–1282.

Erkmen O. and Bozkurt H. (2004) Quality characteristics of retailed sucuk (Turkish dry-fermented sausage). *Food Technol. Biotechnol*. **42,** 63–69.

Favorova O. O., Zargarova T. A., Rukosuyev V. S., Beresten S. F., and Kisselev L. L. (1989) Molecular and cellular studies of tryptophanyl-tRNA synthetases using monoclonal antibodies. Remarkable variations in the content of tryptophanyl-tRNA synthetase in the pancreas of different mammals. *Eur. J. Biochem*. **184,** 583–588.

Fekkes D., van der Cammen T. J., van Loon C. P., et al. (1998) Abnormal amino acid metabolism in patients with early stage Alzheimer dementia. *J. Neural Transm.* **105,** 287–294.

Fischer Y., Thomas J., Kamp J., et al. (1995) 5-hydroxytryptamine stimulates glucose transport in cardiomyocytes via a monoamine oxidase-dependent reaction. *Biochem. J.* **311,** 575–583.

Fletcher P. J. and Paterson I. A. (1989) A comparison of the effects of tryptamine and 5-hydroxytryptamine on feeding following injection into the paraventricular nucleus of the hypothalamus. *Pharmacol. Biochem. Behav*. **32,** 907–911.

Flinn J. P. III. and Edwards R. H. (1998) Multiple residues contribute independently to differences in ligand recognition between vesicular monoamine transporters 1 and 2. *J. Biol. Chem.* **273,** 3943–3947.

Forsstrom T., Tuominen J., and Karkkainen J. (2001) Determination of potentially hallucinogenic N-dimethylated indoleamines in human urine by HPLC/ESI-MS-MS. *J. Scan. J. Clin. Lab. Invest.* **61,** 547–556.

Fromant M., Fayat G., Laufer P., and Blanquet S. (1981) Affinity chromatography of aminoacyl-tRNA syntheses on agarose-hexyl-adenosine-5′-phosphate. *Biochimie* **63,** 541–553.

Gallyas F. (1970) Silver staining of Alzheimer's neurofibrillary changes by means of physical development. *Acta Morphol. Acad. Sci. Hung.* **19,** 1–8.

German D. C., White C. L. 3rd., Sparkman D. R. (1987) Alzheimer's disease: neurofibrillary tangles in nuclei that project to the cerebral cortex. *Neuroscience* **21,** 305–312.

Gilbert J. A., Bates L. A., and Ames M. M. (1995) Elevated aromatic-L-amino acid decarboxylase in human carcinoid tumors. *Biochem. Pharmacol.* **50,** 845–850.

Gomez-Isla T., Hollister R., West H. L., et al. (1997) Neuronal loss correlates with but exceeds neurofibrillary tangles in Alzheimer's disease. *Ann. Neurol.* **41,** 17–24.

Gomes-Ramos P. and Moran M. A. (1998) Ultrastructural aspects of neurofibrillary tangle formation in aging and Alzheimer's disease. *Micros. Res. Tech.* **43,** 49–58.

Gotz J., Schild A., Hoerndli F., and Pennanen L. (2004) Amyloid-induced neurofibrillary tangle formation in Alzheimer's disease: insight from transgenic mouse and tissue-culture models. *Int. J. Dev. Neurosci.* **22,** 453–465.

Hamacher K., Coenen H. H., and Stocklin G. (1986) Efficient stereospecific synthesis of no-carrier added 2-[18F]-fluoro-2-deoxy-D-glucose using aminopolyether supported nucleophilic substitution. *J. Nuclear Med.* **27,** 235–238.

Harris F. M., Brecht W. J., Xu Q., et al. (2003) Carboxyl-terminal-truncated apolipoprotein E4 causes Alzheimer's disease-like neurodegeneration and behavioral deficits in transgenic mice. *Proc. Natl. Acad. Sci. USA* **100,** 10,966–10,971.

Helene C., Dimicoli J. L., and Brun F. (1971) Binding of tryptamine and 5-hydroxytryptamine (serotonin) to nucleic acids. Fluorescence and proton magnetic resonance studies. *Biochemistry* **10,** 3802–3809.

Huang Y., Liu X. Q., Wyss-Coray T., Brecht W. J., Sanan D. A., and Mahley R. W. (2001) Apolipoprotein E fragments present in Alzheimer's disease brains induce neurofibrillary tangle-like intracellular inclusions in neurons. *Proc. Natl. Acad. Sci. USA* **98,** 8838–8843.

Jacob J. and Michaud G. (1962) Effect of 5-hydroxytrptamine and nicotine on hypertension induced by 5-hydroxytryptamine, nicotine, tryptamine and acetaldehyde. *Arch. Int. Pharmacodyn. Ther.* **140,** 92–104.

Jones R. S. (1982) A comparison of the responses of cortical neurones to iontophoretically applied tryptamine and 5-hydroxytryptamine in the rat. *Neuropharmacology* **21,** 209–214.

Juorio A. V. and Durden D. A. (1984) The distribution and turnover of tryptamine in the brain and spinal cord. *Neurochem. Res.* **9,** 1283–1293.

Kalac P. and Krizek M. (2003) A review of biogenic amines and polyamines in beer. *J. Inst. Brew.* **109,** 123–128.

Kalac P., Svecova S., and Pelikanova T. (2002) *Food Chem.* **77,** 349–351.

Kisselev L. L., Favorova O. O., and Kovaleva G. K. (1979) Tryptophanyl-tRNA synthetase from beef pancreas. *Methods Enzymol.* **59 (G),** 234–257.

Lee V. M. -Y., Balin B. J., Otvos L. Jr., and Trojanowski J. Q. (1991) A68: a major subunit of paired helical filaments and derivatized forms of normal tau. *Science* **251,** 675–678.

Levchenko A., Robitaille Y., Strong M. J., and Rouleau G. A. (2004) TAU mutations are not a predominant cause of frontotemporal dementia in Canadian patients. *Can. J. Neurol. Sci.* **31,** 363–367.

Lewin A. H. (2006) Receptors of Mammalian Trace Amines. *The AAPS J.* **8,** E138–E145.

Liberski P. P., Yanagihara R., Gibbs C. J. Jr., and Gajdusek D. C. (1992) Neuronal autophagic vacuoles in experimental scrapie and Creutzfeld-Jacob disease. *Acta Neuropathol.* **83,** 134–139.

Lowe G. and Tansley G. (1984) An investigation of the mechanism of activation of tryptophan by tryptophanyl-tRNA synthetase from beef pancreas. *Eur. J. Biochem.* **138,** 597–602.

Martuscelli M., Crudele M. A., Gardini F., and Suzzi G. (2000) Biogenic amine formation and oxidation by Staphylococcus xylosus strains from artisanal fermented sausages. *Lett. Appl. Microbiol.* **31,** 228–232.

Mattson M. P. and Sherman M. (2003) Perturbed signal transduction in neurodegenerative disorders involving aberrant protein aggregation. *Neuromol. Med.* **4,** 109–132.

McDonald W. M., Holtzheimer P. E., and Byrd E. H. (2006) The diagnosis and treatment of depression in Parkinson's disease. *Curr. Treat Options Neurol.* **8,** 245–255.

Miklossy J., Taddei K., Martins R., et al. (1999) Alzheimer disease: curly fibers and tangles in organs other than brain. *J. Neuropathol. Exp. Neurol.* **58,** 803–814.

Mimnaugh E. G., Xu W., Vos M., et al. (2004) Simultaneous inhibition of hsp 90 and the proteasome promotes protein ubiquitination, causes endoplasmic reticulum-derived cytosolic vacuolization, and enhances antitumor activity. *Mol. Cancer Ther.* **3,** 551–566.

Mizunoya W., Oyaizu S., Hirayama A., and Fushiki T. (2004) Effects of physical fatigue in mice on learning performance in a water maze. *Biosci. Biotechnol. Biochem.* **4,** 827–834.

Molina J. A., Jimenez-Jimenez F. J., Gomez P., et al. (1997) Decreased cerebrospinal fluid levels of neutral and basic amino acids in patients with Parkinson's disease. *J. Neurol. Sci.* **150,** 123–127.

Mousseau D. D. (1993) Tryptamine: a metabolite of tryptophan implicated in various neuropsychiatric disorders. *Matab. Brain Dis.* **8,** 1–44.

Mousseau D. D. and Butterworth R. F. (1994) The [3H]tryptamine receptor in human brain: kinetics, distribution, and pharmacologic profile. *J. Neurochem.* **63,** 1052–1059.

Mousseau D. D. and Butterworth R. F. (1995) Trace amines in hepatic encephalopathy, in *The Progress in Brain Research*, vol. 106, Yu, P. M., Tipton, K. F., and Boulton A. A., eds., Elsevier Science, Amsterdam, pp. 277–284.

Nemecek G. M., Coughlin S. R., Handley D. A., and Moskowitz M. A. (1986) Stimulation of aortic smooth muscle cell mitogenesis by serotonin. *Proc. Natl. Acad. Sci. USA* **83,** 674–678.

Newmester A., Haberler A., Praschak-Rieder N., Willeit M., and Kasper S. (1999) Tryptophan depletion: a predictor of future depressive episodes in seasonal affective disorder? *Int. Clin. Psychopharmacol.* **14,** 313–315.

Nishimura M., Namba Y., Ikeda K., and Oda M. (1992) Glial fibrillary tangles with straight tubulus in the brains of patients with progressive supranuclear palsy. *Neurosci. Lett.* **143,** 35–38.

Novella-Rodriguez S., Veciana-Nogues M. T., Roig-Sagues A. X., Trujillo-Mesa, A. J., and Vidal-Carou M. C. (2002) Influence of starter and nonstarter on the formation of biogenic amine in goat cheese during ripening. *J. Dairy Sci.* **85**, 2471–2478.

O'Kane R. L. and Hawkins R. A. (2003) Na+-dependent transport of large neutral amino acids occurs at the abluminal membrane of the blood-brain barrier. *Am. J. Physiol. Endocrinol. Metab.* **285,** 1167–1173.

Okuyama S., Chaki S., Yoshikawa R., et al. (1997) In vitro and in vivo characterization of the dopamine D4 receptor, serotonin 5-HT2A receptor and alpha-1 adrenoceptor antagonist (R)-(+)-2-amino-4-(4-fluorophenyl)-5-[1-[4-(4-fluorophenyl)-4-oxobutyl] pyrrolidin-3-yl]thiazole (NRA0045). *J. Pharmacol. Exp. Ther.* **282,** 56–63.

Paley E. L. (1997) A mammalian tryptophanyl-tRNA synthetase is associated with protein kinase activity. *Eur. J. Biochem.* **244,** 780–788.

Paley E. L. (1999) Tryptamine-mediated stabilization of tryptophanyl-tRNA synthetase in human cervical carcinoma cell line (1999) *Cancer Lett.* **137,** 1–7.

Paley E. L., Alexandrova N., and Smelansky L. (1995) Tryptophanyl-tRNA synthetase as a human antigen. *Immunol. Lett.* **48,** 201–207.

Paley E. L, Baranov V. N., Alexandrova N. M., and Kisselev L. L. (1991) Tryptophanyl-tRNA synthetase in cell lines resistant to tryptophan analogs. *Exp. Cell Res.* **195,** 66–78.

Paley E. L., Smelyanski L., Malinovskii V., et al. (2006) Mapping and molecular characterization of novel monoclonal antibodies to conformational epitopes on NH_2 and COOH termini of mammalian tryptophanyl-tRNA synthetase reveal link of the epitopes to aggregation and Alzheimer's disease. *Mol. Immunol.* In press.

Perani D., Bressi S., Cappa S. F., et al. (1993) Evidence of multiple memory systems in the human brain. A [18F]FDG PET metabolic study. *Brain* **116,** 903–919.

Porter R. J., Lunn B. S., and O'Brien J. T. (2003) Effects of acute tryptophan depletion on cognitive function in Alzheimer's disease and in the healthy elderly. *Psychol. Med.* **33,** 41–49.

Riederer P., Danielczyk W., and Grunblatt E. (2004) Monoamine oxidase-B inhibition in Alzheimer's disease. *Neutoxicology* **25,** 271–277.

Rosenblum W. I. (1999) The presence, origin, and significance of A beta peptide in the cell bodies of neurons. *J. Neuropathol. Exp. Neurol.* **58,** 575–581.

Rowe S. K. and Rapaport M. H. (2006) Classification and treatment of sub-threshold depression. *Curr. Opin. Psychiatry* **19,** 9–13.

Rubin B. Y., Anderson S. L., Xing L., Powell R., and Tate W. P. (1991) Interferon induces tryptophanyl-tRNA synthetase expression in human fibroblasts. *J.Biol. Chem.* **266,** 24,245–24,248.

Sari Y. and Zhou F. C. (2004) Prenatal alcohol exposure causes long-term serotonin neuron deficit in mice. Alcoholism: clinical and experimental research. *Alcohol Clin. Exp. Res.* **28,** 941–948.

Shalaby A. R. (2000) Changes in biogenic amines in mature and germinating legume seeds and their behavior during cooking. *Nahrung* **44,** 23–27.

Spillantini M. G. and Goedert M. (1998) Tau protein pathology in neurodegenerative diseases. *Trends Neurosci.* **21,** 428–433.

Smith G., Vigen V., Evans J., Fleming K., and Bohac D. (1998) Patterns and associates of hyperphagia in patients with dementia. *Neuropsychiatr. Neuropsychol. Behav. Neurol.* **11,** 97–102.

Sokolova O., Accardi A., Gutierrez D., Lau A., Rigney M., and Grigorieff N. (2003) Conformational changes in the C terminus of Shaker K+ channel bound to the rat Kvbeta2-subunit. *Proc. Natl. Acad. Sci. USA* **100,** 12,607–12,612.

Starkstein S. E., Jorge R., Mizrahi R., and Robinson R. G. (2005) The construct of minor and major depression in Alzheimer's disease. *Am. J. Psychiatry* **162,** 2086–2093.

Sugimoto Y., Kimura I., Yamada J., Watanabe Y., and Horisaka K. (1994) Effects of tryptamine on plasma glucagon levels in mice. *Neurochem. Res.* **19,** 15–18.

Sugimoto Y., Kimura I., Yamada J., Watanabe Y., Takeuchi N., and Horisaka K. (1991) The involvement of insulin in tryptamine-induced hypoglycemia in mice. *Life Sci.* **48,** 1679–1683.

Sullivan J. L., Coffey C. E., Basuk B., Cavenar J. O., Maltbie A. A., and Zung W. W. (1980) Urinary tryptamine excretion in chronic schizophrenics with low platelet MAO activity. *Biol. Psychiatry* **15,** 113–120.

Tabaton M., Cammarata S., Mancardi G., et al. (1991) Ultrastructural localization of beta-amyloid, tau, and ubiquitin epitopes in extracellular neurofibrillary tangles. *Proc. Natl. Acad. Sci. USA* **88,** 2098–2102.

Taylor M. W. and Feng G. S. (1991) Relationship between interferon-gamma, indoleamine 2,3-dioxygenase, and tryptophan catabolism. *FASEB J.* **11,** 2516–2522.

Thomas J. C., Saleh E. F., Alammar N., and Akroush A. M. (1998) The indole alkaloid tryptamine impairs reproduction in Drosophila melanogaster. *J. Econ. Entomol.* **91,** 841–846.

Tsuchiya H., Ohtani S., Yamada K., Tajima K. and Sato M. (1995) Formation of tetrahydro-beta-carbolines in human saliva. *Biochem. Pharmacol.* **50,** 2109–2112.

Tuzikov F. V., Tuzikova N. A., Vavilin V. I., et al. (1991) Aggregation of tryptophanyl-tRNA synthetase depending on temperature. Study by a low-angle scatter X-ray method. *Mol. Biol. (Mosk)* **25,** 740–751.

Valls J. E., Bello R. A., and Kodaira M. S. (2002) Semiquantitative analysis by thin-layer chromatography (TLC) of biogenic amines in dried, salted and canned fish products. *J. Food Qual.* **26,** 91–180.

von Gunten A., Kovari E., Bussiere T., et al. (2006) Cognitive impact of neuronal pathology in the entorhinal cortex and CA1 field in Alzheimer's disease. *Neurobiol. Aging* **27,** 270–277.

Walter J., Hertel C., Tannock G. W., Lis C. M., Munro K., and Hammes W. P. (2001) Detection of Lactobacillus, Pediococcus, Leuconostoc, and Weissella species in human feces by using group-specific PCR primers and denaturing gradient gel electrophoresis. *Appl. Environ. Microbiol.* **67,** 2578–2585.

Weiner M. F., Hynan L. S., Parikh B., et al. (2003) Can Alzheimer's disease and dementias with Lewy bodies be distinguished clinically? *J. Geriatr. Psychiatr. Neurol.* **16,** 245–250.

Yamada J., Sugimoto Y., and Horisaka K. (1987a) The behavioral effects of intravenously administered tryptamine in mice. *Neuropharmacology* **26,** 49–53.

Yamada J., Wakita H., Sugimoto Y., and Horisaka K. (1987b) Hypothermia induced in mice by intracerebroventricular injection of tryptamine: involvement of the 5-HT1 receptor. *Eur. J. Pharmacol.* **139,** 117–119.

Yoshida M., Goto K., and Watanabe S. (2001) Task-dependent strain difference of spatial learning in C57BL/6N and BALB/c mice. *Physiol. Behav.* **73,** 37–42.

Young E. A., Neff N. H., and Hadjiconstantinou M. (1994) Phorbol ester administration transiently increases aromatic L-amino acid decarboxylase activity of the mouse striatum and midbrain. *J. Neurochem.* **63,** 694–697.